(2)

NAVAL POSTGRADUATE SCHOOL
Monterey, California

THESIS

LITHIUM ION SOURCE
FOR SATELLITE CHARGE CONTROL

by

Song, Tae Ik

June 1990

Thesis Advisor Richard C. Olsen

68

REPORT DOCUMENTATION PAGE

1a Report Security Classification: Unclassified	1b Restrictive Markings
2a Security Classification Authority	3 Distribution Availability of Report: Approved for public release; distribution is unlimited.
2b Declassification Downgrading Schedule	
4 Performing Organization Report Number(s)	5 Monitoring Organization Report Number(s)
6a Name of Performing Organization: Naval Postgraduate School; 6b Office Symbol (*if applicable*): 61	7a Name of Monitoring Organization: Naval Postgraduate School
6c Address (*city, state, and ZIP code*): Monterey, CA 93943-5000	7b Address (*city, state, and ZIP code*): Monterey, CA 93943-5000
8a Name of Funding Sponsoring Organization; 8b Office Symbol (*if applicable*)	9 Procurement Instrument Identification Number
8c Address (*city, state, and ZIP code*)	10 Source of Funding Numbers: Program Element No; Project No; Task No; Work Unit Accession No

11 Title (*include security classification*): LITHIUM ION SOURCE FOR SATELLITE CHARGE CONTROL

12 Personal Author(s): Song, Tae Ik

13a Type of Report	13b Time Covered	14 Date of Report (*year, month, day*)	15 Page Count
Master's Thesis	From To	June 1990	60

16 Supplementary Notation: The views expressed in this thesis are those of the author and do not reflect the official policy or position of the Department of Defense or the U.S. Government.

17 Cosati Codes			18 Subject Terms (*continue on reverse if necessary and identify by block number*)
Field	Group	Subgroup	Lithium Ion Source, Satellite Charge Control

19 Abstract (*continue on reverse if necessary and identify by block number*)

A lithium ion source using thermal emission from mineral β-eucryptite has been investigated as a possible control device for spacecraft charging. This source can be used for control of positively charged spacecraft potentials in sunlight and differentially charged spacecraft surfaces in shadow. This thesis investigates the dependence of the emitted ion current on several parameters: source temperature (power input), source bias potentials and potentials applied to simulated spacecraft geometries. Saturation currents of about 5.8 μA were measured at an extraction potentials of 100 Volts from a source of 0.317 cm^2 surface area with a power input of 18 Watts. The lifetime due to ion exhaustion was found to be approximately 200 hours for this compact source. Our results indicate that this type of ion source may represent an effective charge control device for spacecraft.

20 Distribution Availability of Abstract	21 Abstract Security Classification	
☒ unclassified unlimited ☐ same as report ☐ DTIC users	Unclassified	
22a Name of Responsible Individual: Richard C. Olsen	22b Telephone (*include Area code*): (408)646-2019	22c Office Symbol: 61Os

DD FORM 1473,84 MAR — 83 APR edition may be used until exhausted. All other editions are obsolete — security classification of this page

Approved for public release; distribution is unlimited.

Spacecraft Charge Control
Using a Lithium Ion Source

by

Song,Tae Ik
Captain, Korean Army
B.S., Korea Military Academy, 1983

Submitted in partial fulfillment of the
requirements for the degree of

MASTER OF SCIENCE IN PHYSICS

from the

NAVAL POSTGRADUATE SCHOOL
June 1990

Author: 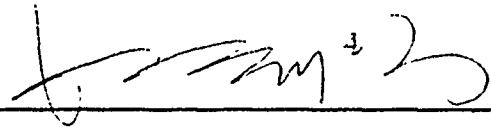

Song,Tae Ik

Approved by: 

Richard C. Olsen, Thesis Advisor

Otto Heinz, Second Reader

Karlheinz E. Woehler, Chairman,
Department of Physics

ABSTRACT

A lithium ion source using thermal emission from mineral β-eucryptite has been investigated as a possible control device for spacecraft charging. This source can be used for control of positively charged spacecraft potentials in sunlight and differentially charged spacecraft surfaces in shadow. This thesis investigates the dependence of the emitted ion current on several parameters: source temperature (power input), source bias potentials and potentials applied to simulated spacecraft geometries. Saturation currents of about 5.8 μA were measured at an extraction potentials of 100 Volts from a source of 0.317 cm^2 surface area with a power input of 18 Watts. The lifetime due to ion exhaustion was found to be approximately 200 hours for this compact source. Our results indicate that this type of ion source may represent an effective charge control device for spacecraft.

TABLE OF CONTENTS

LIST OF FIGURES

I. INTRODUCTION

A. NEED FOR CHARGE CONTROL

Charging of the outer surface or entire structure of a spacecraft in orbit can have a severe impact on satellites and the scientific output of satellite instruments. Spacecraft charging is the development of a potential difference between a spacecraft and its plasma environment. There are three main cases of charging on geosynchronous satellites. The first is negative charging in eclipse. Typical values for spacecraft potential in eclipse are from -1 to -10 KV. This results in current flows as shown in Figure 1a. The remaining two cases involve sunlight conditions. Figure 1b shows the situation in sunlight outside the plasmasphere when photoemission is relatively important. An equilibrium potential is achieved when the flow of escaping photoelectrons is equal to the difference between the flows of plasma electrons and ions which reach the surface. In order to fulfil this condition the potential of the surface must be positive and a significant fraction of the emitted photoelectrons must return to the surface. [Ref.1]

Considering further the case of a spacecraft in sunlight, Figure 2a illustrates the situation of a body with a conductive and equipotential surface when photoemission is predominant. On the shadowed side of the spacecraft plasma ion and electron currents are the only contributors; on the sunlight side photoemission plays an important role. As long as the total photoelectron current emitted on one side exceeds the difference between plasma electron and ion currents collected on both sides, the satellite charges to a positive potential. The magnitude of the charge is governed by the mean photoelectron energy and is of the order of few volts. Figure 2b represents a satellite with an insulating surface (SiO_2) in sunlight. The current exchange on the sunlight side remains unchanged. For the shadowed side, however, the incoming electron plasma cur-

rent cannot be conducted across the surface to the front side and be released by photoemission. So the dark side will adopt a negative potential. The magnitude of potential in the plasma sheet is a negative potential which can vary from -100 V to -1 KV. [Ref.1]

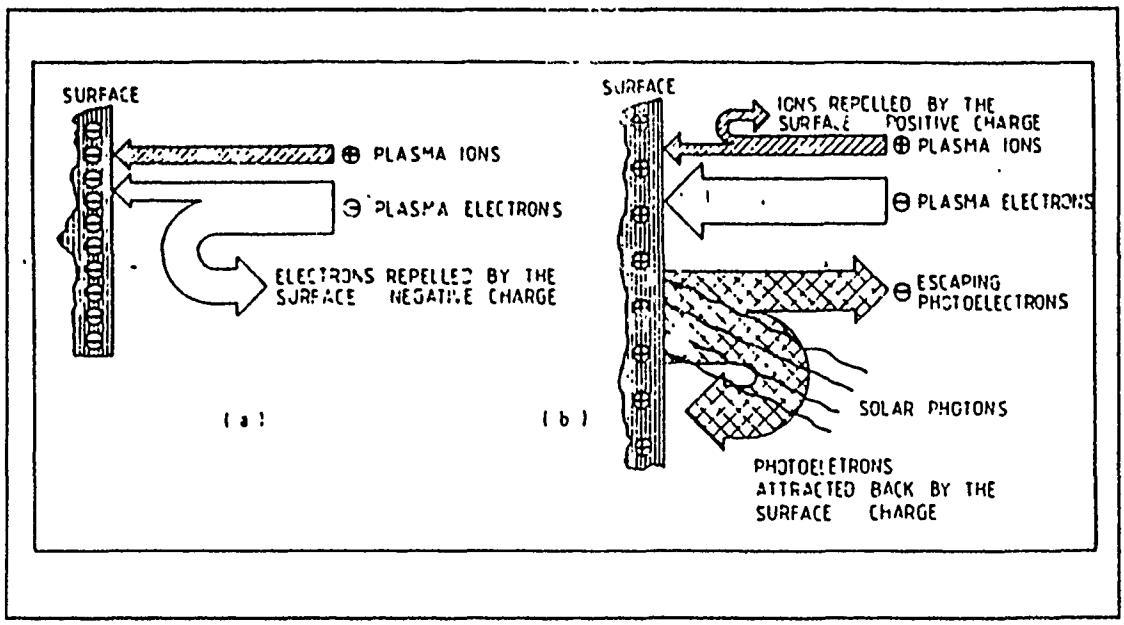

Figure 1. Qualitative illustration of the charging: of a surface by a plasma. (a)Surface in shadow(b) Surface in sunlight [Ref.1]

The importance of this form of differential charging is that it can lead to arcing on the satellite surface. Discharges on charged spacecraft generally occur between the structure and surface elements, with an opposite polarity. These discharges can cause failure of the measurement system and command system on scientific satellites. Control of spacecraft potentials, therefore, has substantial value for satellites. This thesis work presents a technique for controlling the body potential (positively or differentially charged) experimentally using a lithium ion emitter developed by O. Heinz and R.T. Reaves in 1968. [Ref.2]

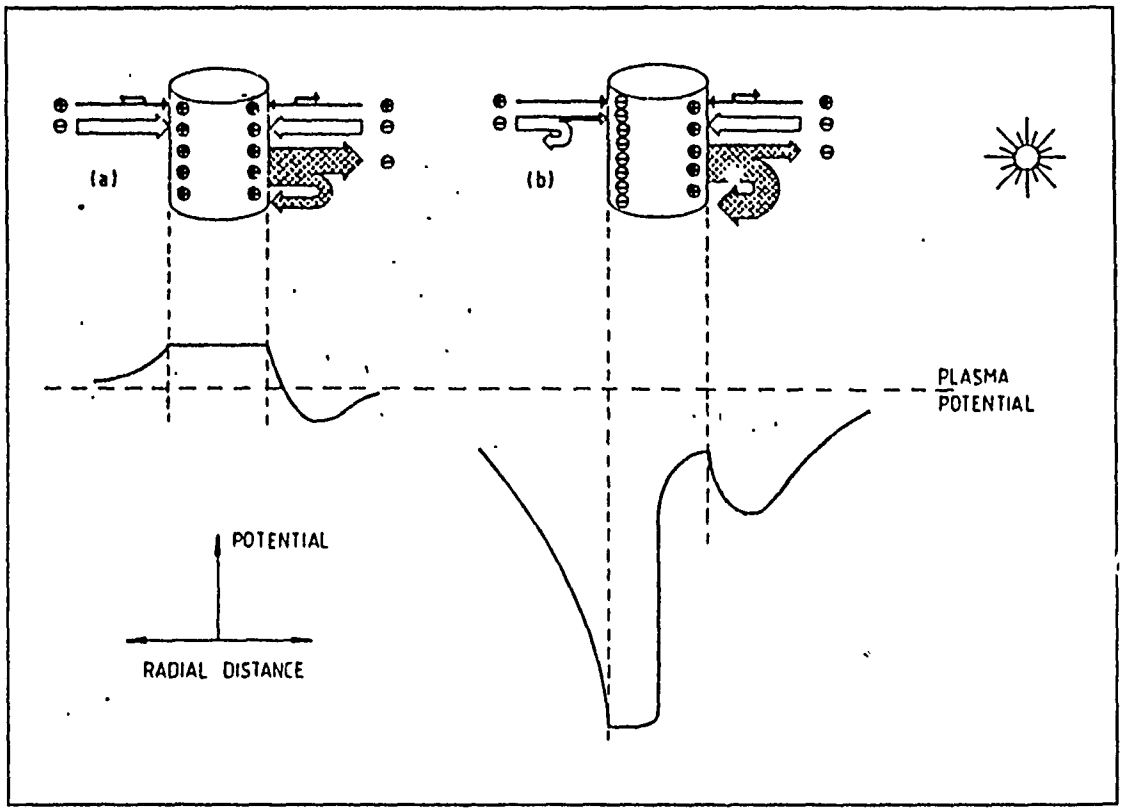

Figure 2. Schematic representation of particle flows.: (a)a conductive surface (b) an insulator surface. [Ref.1]

B. PREVIOUS APPROACHES

1. Electron Sources

The history of flight experiments in charge control is brief. The primary experiments were conducted on the geosynchronous ATS-5 and ATS-6 satellites, and the near-geosynchronous P78-2 (SCATHA) satellite. [Ref.3,4]

ATS-5 carried filament electron sources as part of an ion engine experiment. The electron emitter on ATS-5 was operated hundreds of times over a 4-year period, primarily during eclipses. These operations succeed in reducing the magnitude of the negative potentials on the satellite, but rarely discharged the spacecraft completely as

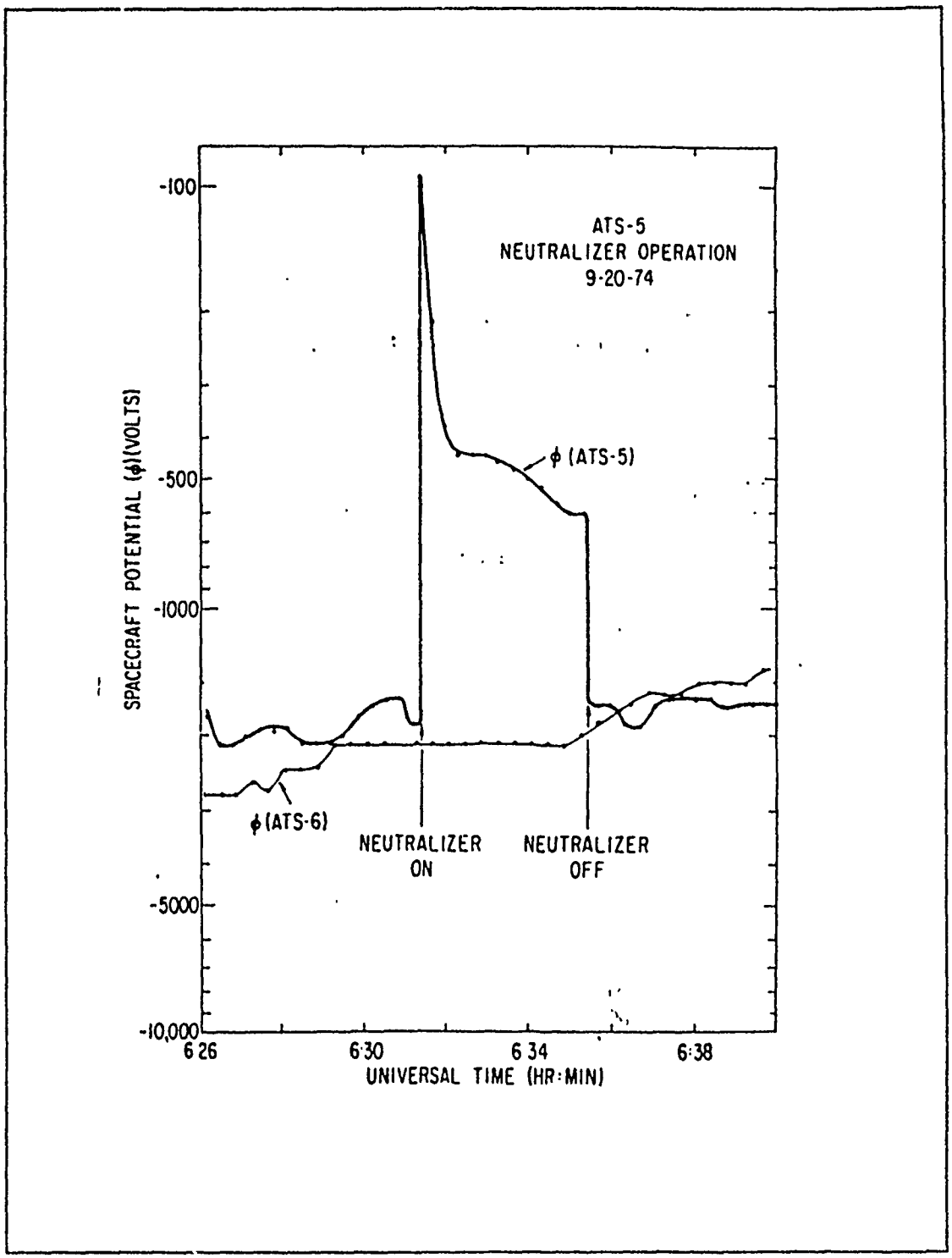

Figure 3. ATS-5 neutralizer operation, September 20, 1974[Ref.4]

shown in Figure 3. Transient negative potentials of greater size than the eclipse equilibrium value were seen when the neutralizer was switched off as shown on Figure 4. Modeling of the current balance to the spacecraft showed that less than 1 percent of the emitter current was escaping the spacecraft at equilibrium. Three-dimensional modeling of the potentials and currents with NASA Charging Analyzer Program (NASCAP) showed the development of differential potentials on the order of 100 V to be developed on the spacecraft surfaces, limiting the emission of the filament. The limitations was sufficient to explain the equilibrium potentials seen and would apply to most spacecraft with insulating surfaces.

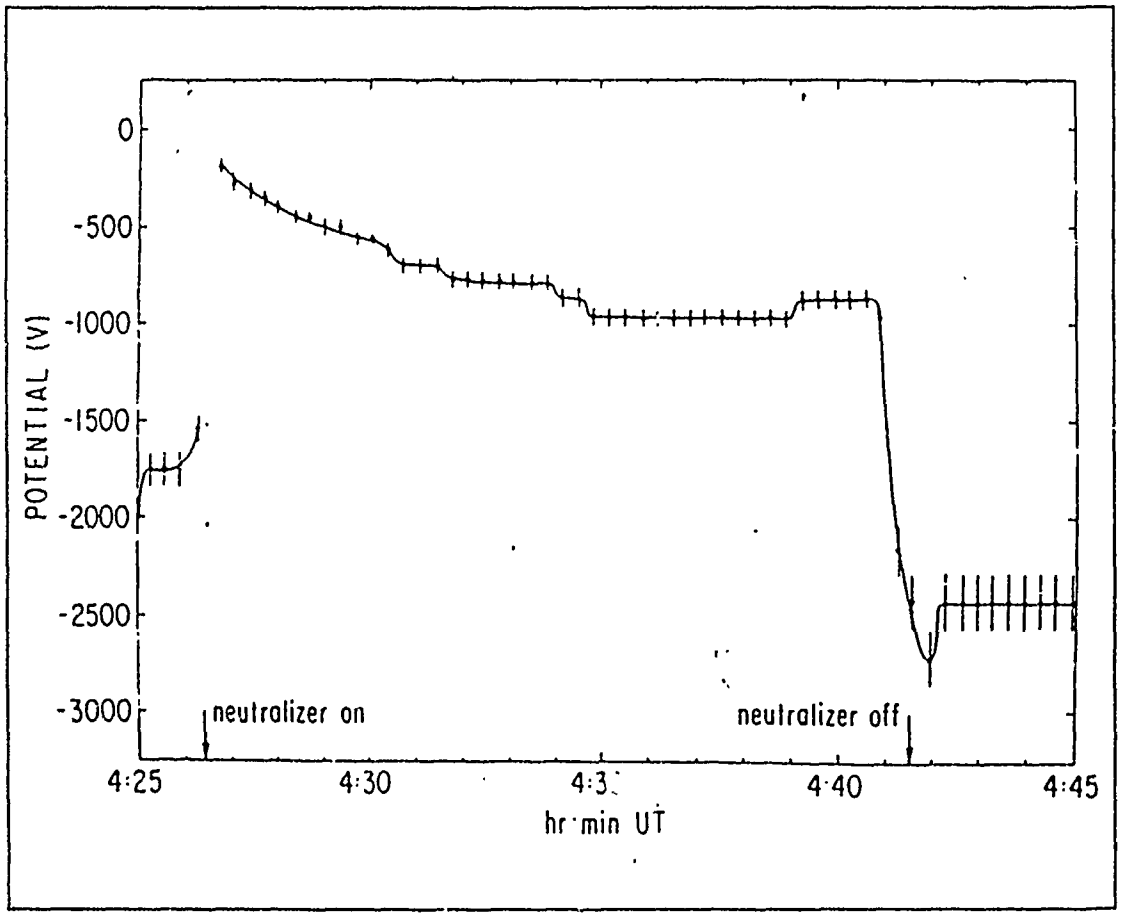

Figure 4. ATS-5 neutralizer operation, March 28, 1978 [Ref.4]

The experience obtained with ATS-5 data and modeling were directly applicable to the data obtained from the electron gun experiments on the SCATHA satellite with a more powerful electron source. The SCATHA satellite generally was similar to ATS-5, i.e., cylindrical,and dominated by insulating surfaces. The electron emitter was considerably more sophisticated, however. The experimental results from SCATHA were similar to the ATS-5 results qualitatively. Electron emission initially caused to satellite potential to rise toward zero, but limiting processes prevented the full electron beam from escaping. The satellite did not necessarily discharge any further with increasing current and voltage. Those operations confirmed the need to provide a means of discharging the dielectric surfaces, since increasing the electron gun accelerating voltage will only increase the magnitude of the differential potentials on the spacecraft surface. [Ref.4]

2. Plasma Sources

a. Ion Engine

An ion engine is a device which combines an ion beam with a charge and current balancing electron source. The ion engine operations on Applied Technology Satellite 6 (ATS-6) altered the charge state of the spacecraft, changing the spacecraft potentials with respect to the distant plasmas. Plasma emission in quiet environments (plasma temperatures below 1 kilovolt) caused the spacecraft potential to shift from a few volts positive to a few volts negative. A net ion current is emitted in such cases. The emission of a plasma or beam in energetic environments (plasma temperatures in the 5 - 10 KeV range) in sunlight caused larger changes. Typical equilibrium potentials with the engine off for ATS-6 in such environments were on the order of a hundred volts negative, with variations in potential across the spacecraft surface of comparable magnitude. Engine operations under such conditions raised the mainframe potential to near zero volts, and discharged the differential potentials on the dielectric surfaces.

Plasma emission by the plasma bridge neutralizer was an effective method of discharging kilovolts potentials in eclipse. Figure 5 shows the plasma bridge operation for eclipse discharge. This illustrated that plasma emission was the preferred way for controlling satellite charging.[Ref.5]

b. Hollow Cathode

The success of plasma sources in controlling satellite charging have led to their continued development for charge control. A hollow cathode based plasma source will be flown on the NASA POLAR satellite, to be launched in 1992. The problem with this technology is that it is heavy (10 - 20 Kg payload weight), uses large amounts of power (10 - 20 W), and is electromagnetically noisy. These problems motivate a continued effort to find alternate forms of charge control technology.

C. LITHIUM ION SOURCE

1. Basic Concept and Theory

The lithium ion emitters which used in our experiment were developed by Otto Heinz and R.T. Reaves in 1968. To be familiar with this lithium ion emitter we will study the general physical properties and preparation of crystalline compounds $Li_2O \cdot Al_2O_3 \cdot 2SiO_2$ which is known as β-eucryptite.

a. Structure of Beta-eucryptite

Beta-eucryptite is one of the aluminosilicates. The crystal structure, shown in Figure 6, is similar to the high-temperature quartz structure, yet differs from it in that half of the silicon atoms are replaced by aluminum atoms in alternate layers along the c-axis. The lithium ions are in the interstitial space on the level where the substitution takes place, surrounded by four oxygen atoms. This arrangement has a very satisfactory Pauling electrostatic bond structure. The oxygens surrounding the Li are shared by one Si and one Al, so that they receive electrostatic bonds of strength 1 3/4 from this source. The tetrahedrally coordinated Li atoms contribute the remaining 1/4.

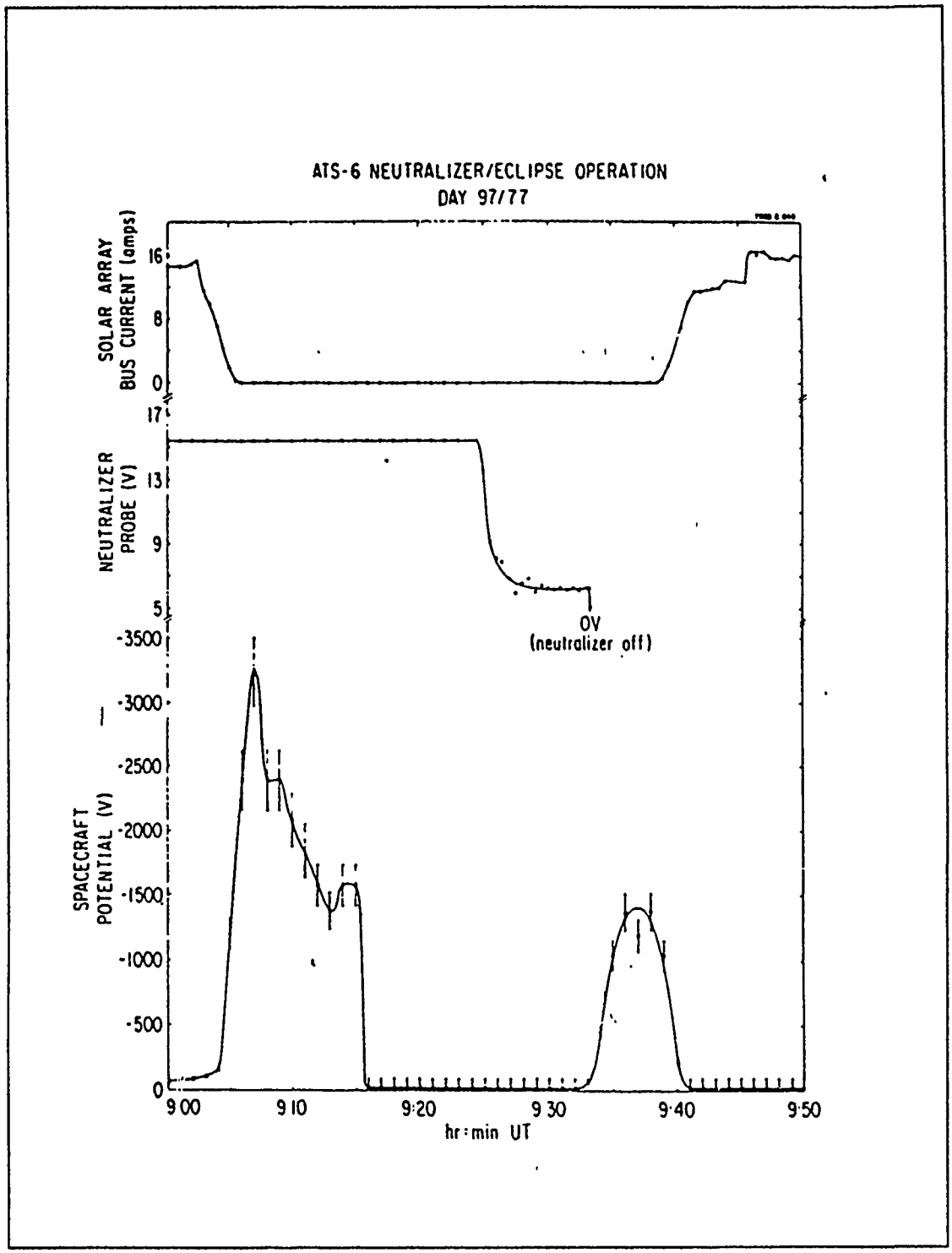

Figure 5. Plasma bridge operation, April 7, 1977 [Ref.5]

Beta-eucryptite is extremely anisotopic in thermal expansion, with coefficients of thermal expansion in the a and c crystallographic directions of $+82 \times 10^{-7}$ and $-176 \times 10^{-7} per^{\circ}C$, respectively. The net effect of this anisotropic expansion is to enlarge the openings of the crystal lattice in which the lithium ions are situated. This is the reason why lithium ions are readily emitted from this type of crystal structure if the material is sufficiently heated. [Ref.6]

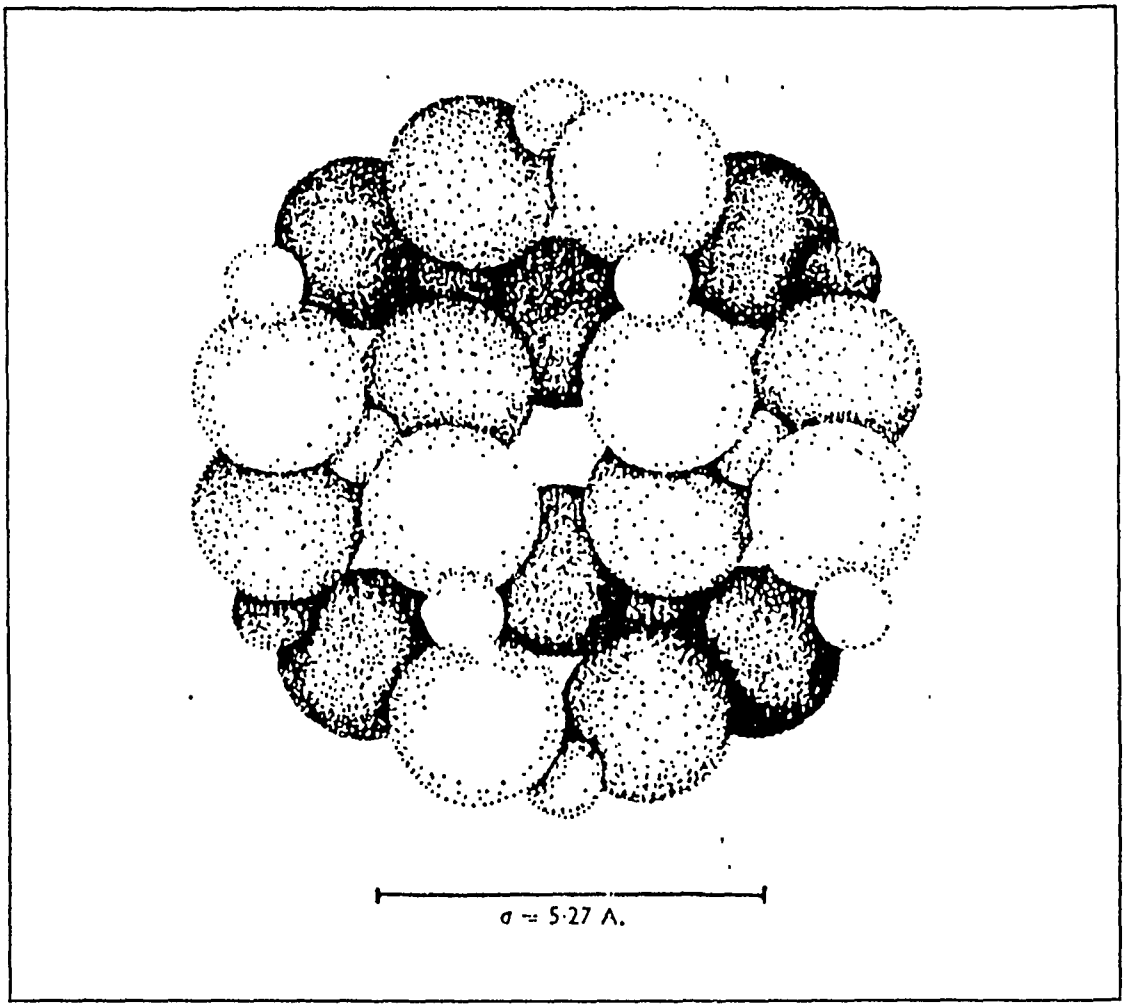

Figure 6. **Crystal structure of β-eucryptite viewed along c axis.:** Large spheres represents oxygen atoms, small spheres either Si or Al atoms. The lithium ions are situated in center opening. [Ref.6]

Samuel K. Allison and M. Kamegai explained about the technique for the preparation of artificial β-eucryptite. It can be synthesized by heating as following formula. [Ref.6,7]

$$Li_2CO_3 + 2SiO_2 + Al_2O_3 \overset{heat}{\rightarrow} Li_2O \cdot Al_2O_3 \cdot 2SiO_2 + CO_2\uparrow \qquad (0)$$

b. Lithium Ion Emission

J. P. Blewett and E. J. Jones were among the first to recognize the excellent ion-emission properties of β-eucryptite and in fact hypothesized that in the crystal lattice the lithium ions are situated in large "holes". The alkali ion is therefore comparatively free to migrate within the lattice, and with the aid of small electrolytic potentials which are bound to be present, it migrates to the surface and is emitted easily as indicated by the work function. The work function for ions determined by F. M. Johnson on a large number of samples of sintered β-eucryptite were all in the neighborhood of 2.0 eV in contrast to 2.7-4.0 eV as determined by Blewett and Jones. [Ref.8]

Fred M. Johnson studied ion emission by means of simple diode structures with an emitter collector spacing of about 1 millimeter. The ion emission data could be fitted to a Schottky-type equation:

$$\log_{10} I_s = \log_{10} I_{so} + \frac{1.9}{T_s}\left(\frac{V}{d}\right)^{1/2} \qquad (1)$$

where V is measured in volts, d in centimeters, I_{so} is the saturated ion emission current at zero biased voltage, and T_s is the apparent Schottky temperature. The second term in Equation (1) arises from the fact that an ion induces an image charge in the material as it leaves the surface and hence modifies the potential distribution immediately outside the material. The values of Schottky temperature, T_s, range from 210 to 430°K depending

on the emitter temperature, whereas the actual temperature of the ion emitter was in the 1300 to 1600°K range.

The ion-emission data in the high-voltage region and 1300 to 1600 °K temperature range may be fitted to the following equation, for a 50% lithium sample:

$$\log_{10} I_s = \log_{10} I_{so} + \frac{1.9}{1375 - 0.726T} \left(\frac{V}{d}\right)^{1/2} \qquad (2)$$

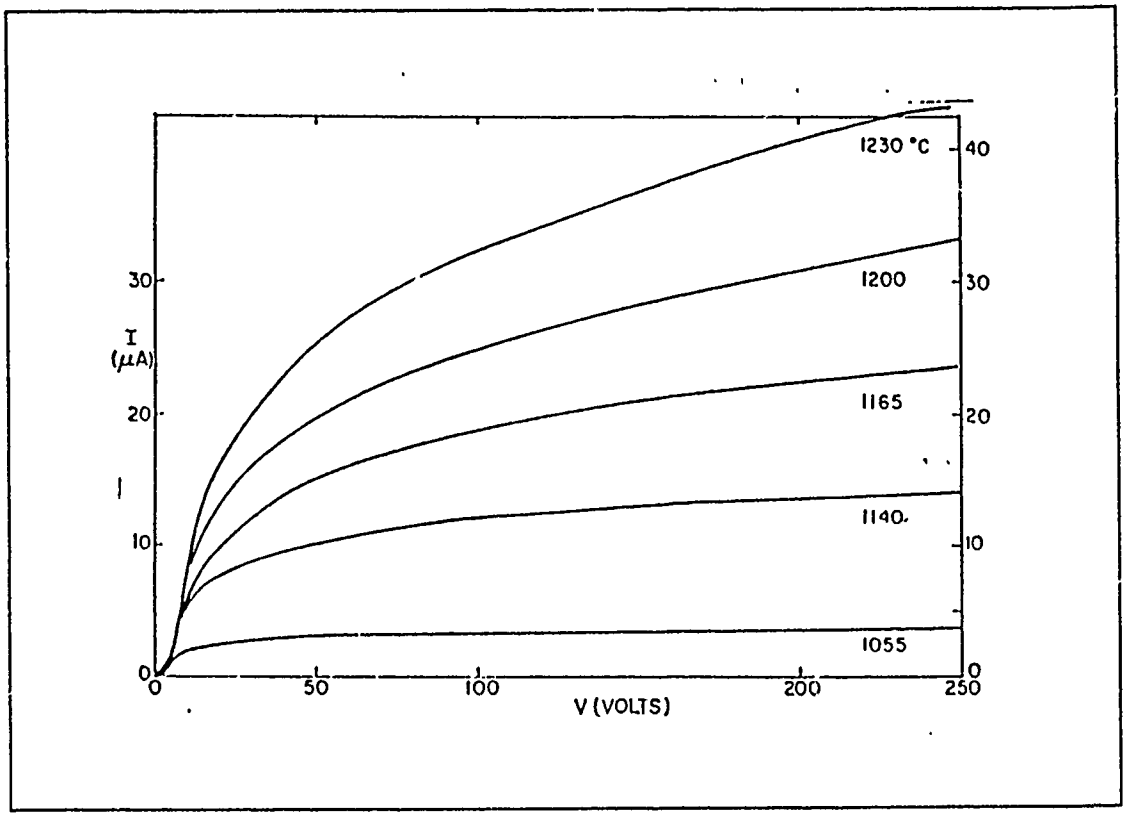

Figure 7. Typical diode characteristics of current vs voltage. [Ref.6]

Figure 7 shows the I-V diode characteristics for a sample which had 50% lithium composition, 50% inert materials. [Ref.6]

In the low-voltage region, the lithium ion emission should be space-charge limited, meaning that the ion current is governed by the Child-Langmuir equation:

$$I = 2.33 \times 10^{-6} \frac{V^{3/2} S}{d^2} \sqrt{\frac{m}{M}} \quad Amperes \tag{3}$$

or

$$j = 2.33 \times 10^{-6} \frac{V^{3/2}}{d^2 (1823.3M)^{1/2}} \quad Amps/cm^2 \tag{4}$$

where m/M is the ratio of the electron mass to the ion mass, d is the electrode spacing in centimeters and S is the emitting area of source in cm^2. This is the appropriate form for calculating the space-charge-limited current for the lithium ion source used in our experiments. A typical graph of I versus V is shown in Figure 8. In the space-charge-limited region, the experimental points are expected to lie on the theoretical curve, which is drawn as a dashed line in Figure 8 and marked "perveance" line. The deviations from the straight line are interpreted as being due to the resistance of the thermionic emitter. The ion current is then given by

$$I = P(V - IR)^{3/2} \tag{5}$$

where P is the perveance of the diode, i.e.,

$$P = \frac{2.33 \times 10^{-6} S}{d^2} \sqrt{\frac{m}{M}} \tag{6}$$

V is the plate voltage, and R is the initial resistance of the ion emitter. [Ref.6,9]

2. Lithium Ion Emitter for Low Energy Beam Experiments

Up to now we learned about the fact that the crystalline compounds $Li_2O \cdot Al_2O_3 \cdot 2SiO_2$ (β-eucryptite) will emit Li^+ ions when heated above 1000°C. We now consider the implementation of a compact Li^+ emitter particulary suited for low energy experiments ($E \lesssim 100eV$) which will be used for this work.

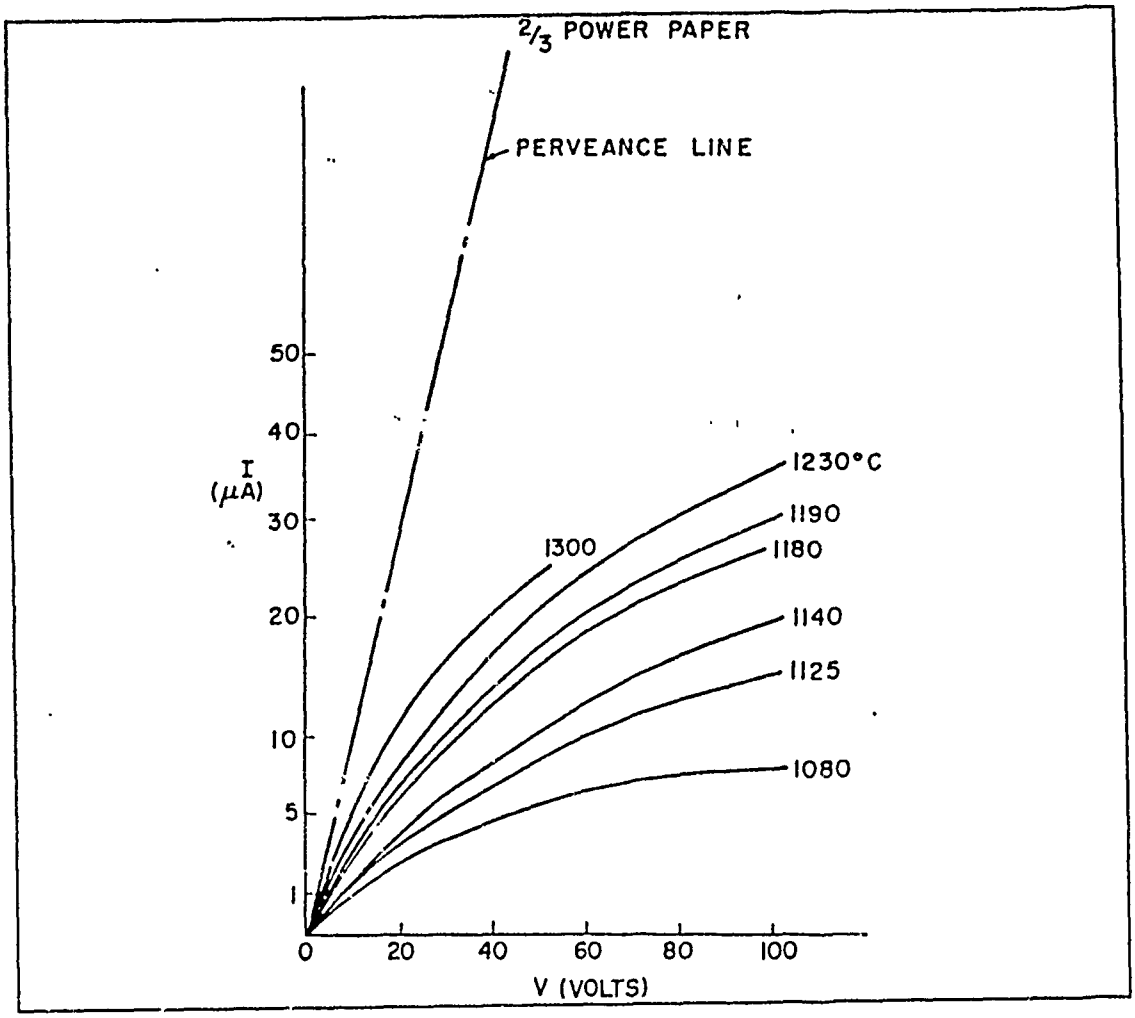

Figure 8. Typical plot of $I^{2/3}$ versus V for a lithium ion emitter.: The perveance line applies to the Child-Langmuir equation. [Ref.6]

Figure 9 shows the emitter consisting of an indirectly heated, highly porous, tungsten plug into which the emitter material has been placed. The molybdenum body holding the plug is machined with a solid partition for complete isolation between the emitter and the heater cavity. The three rhenium support struts are brazed at a 120° spacing with a moly/ruthenium eutectic at 1200°C in hydrogen, yielding a ductile and versatile mounting tripod. The heater is a noninducting wound bipolar coil with heliarc

welded rhenium leads solidly potted into the body cavity. The high purity Al_2O_3 potting mix is H_2 fired at 1900°C which completely immobilizes the heater. The emitter matrix, a specially prepared, extremely porous, tungsten disc with a density of 30% (70% porosity) is heliarc welded to the moly body. The β-eucryptite powder is placed on the face in controlled amounts and melted into the porous disc at approximately 1650°C in a hydrogen atmosphere.

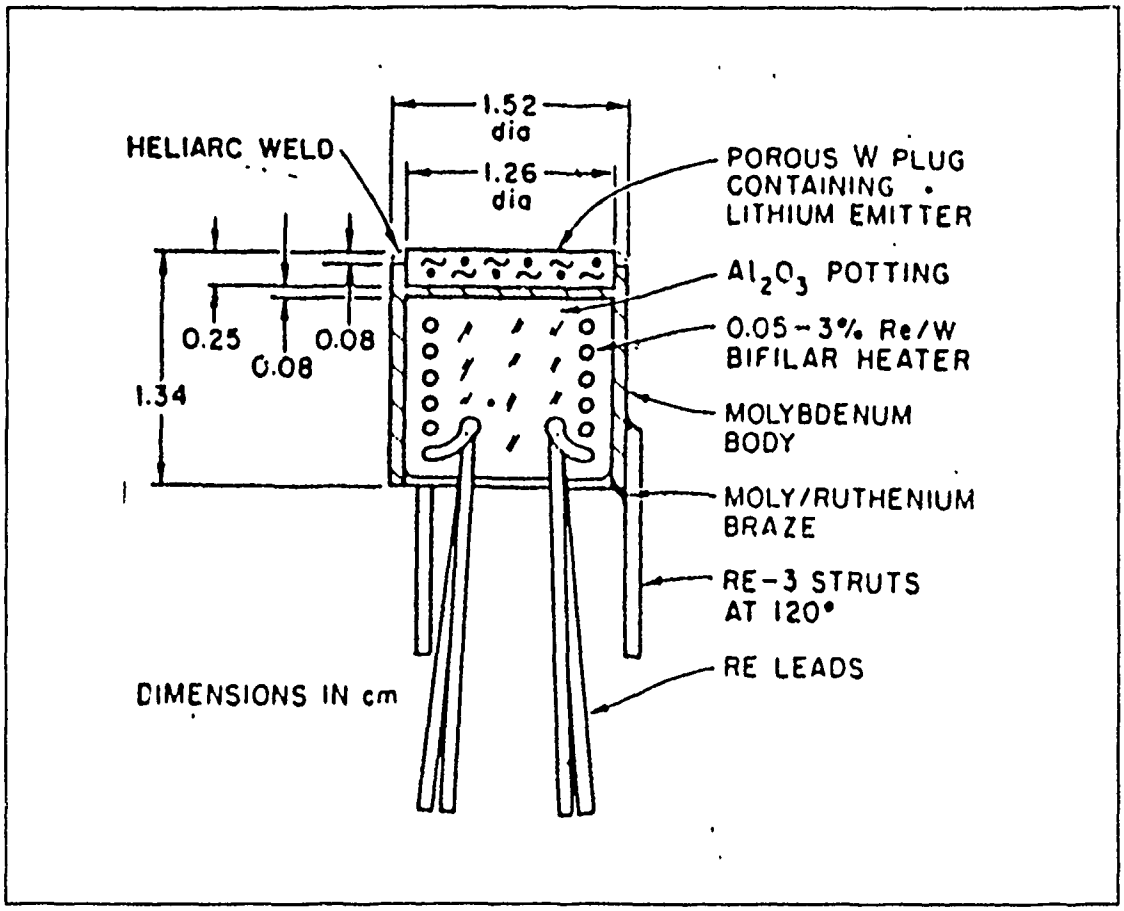

Figure 9. Construction of Lithium Ion Emitter. [Ref.2]

Figure 10 shows the observed total emission current as a function of emitter power and emitter surface temperature for a 1.52 cm diameter source. Although the currents are small they are more than adequate for most low energy beam experiments

where space charge limitations usually restrict the beam to lower values than those shown on Figure 10. A mass analysis of the beam indicated that there were small amounts of oth r akali ions present (~ 1%) when the emitter is fired up, but that after a few hours of running the impurities decreases to about 0.01% resulting in a lithium ion beam of very high purity. The lifetime of the $^6Li^+$ ion emitter was about 200h without any observable deterioration. [Ref.2,10]

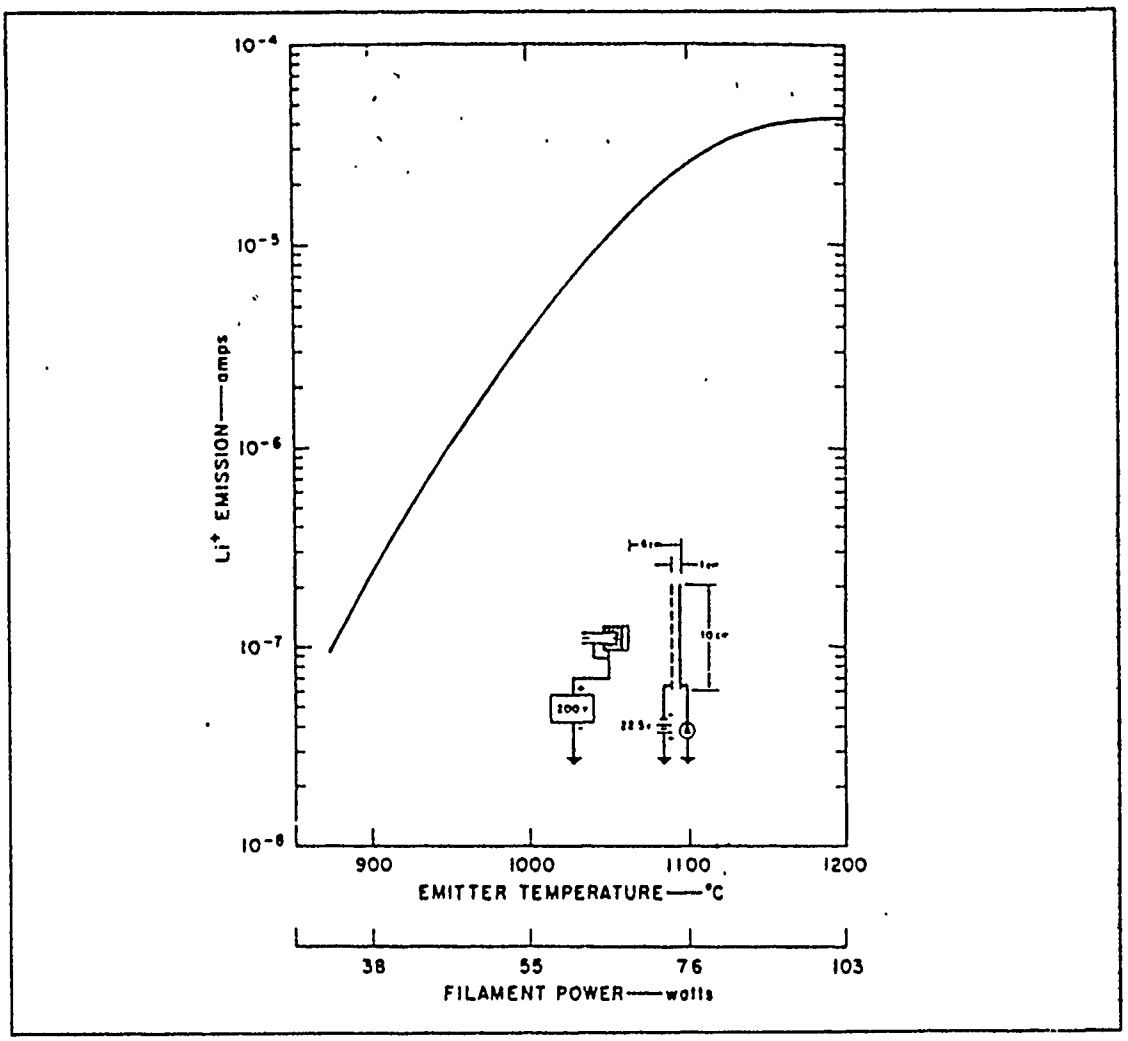

Figure 10. **Total emission current as a function of input power(Temp.).:** Insert shows experimental arrangement. [Ref.2]

3. Other Designs

There are a few other methods of creating a low energy ion source which are worth mentioning.

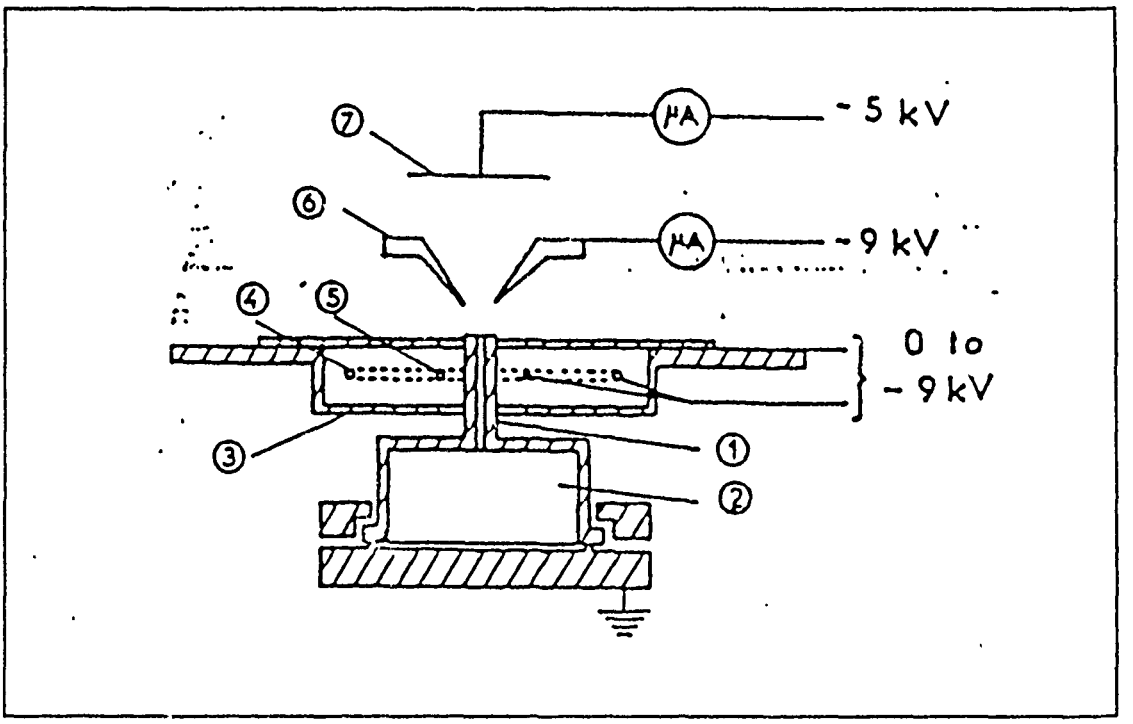

Figure 11. **Cross section of the lithium capillary ion source:** (1)Capillary tube, (2)lithium reservoir, (3)electron reflector, (4)Hot tungsten filament, (5)cold filament, (6)extractor, (7)collector. [Ref.11]

M. Remy and R.Haug constructed a capillary ion source using the surface ionization of lithium on rhenium in 1969. Figure 11 shows the cross section of the lithium capillary ion source. The utilization of surface ionization for the production of Li^+ ions has some advantages. The life of the ion source is limited only by the capacity of the lithium reservoir. The emitted ionic current can only be large if the metallic emitting surface has a high work function. Using a heat reflector around the reservoir, the temperature of the lithium reservoir can be increased as shown in Figure 11. With the

capacity of lithium reservoir 0.5g, currents of 400 μA was obtained during 300h, and 100 μA during 1000h. [Ref.11]

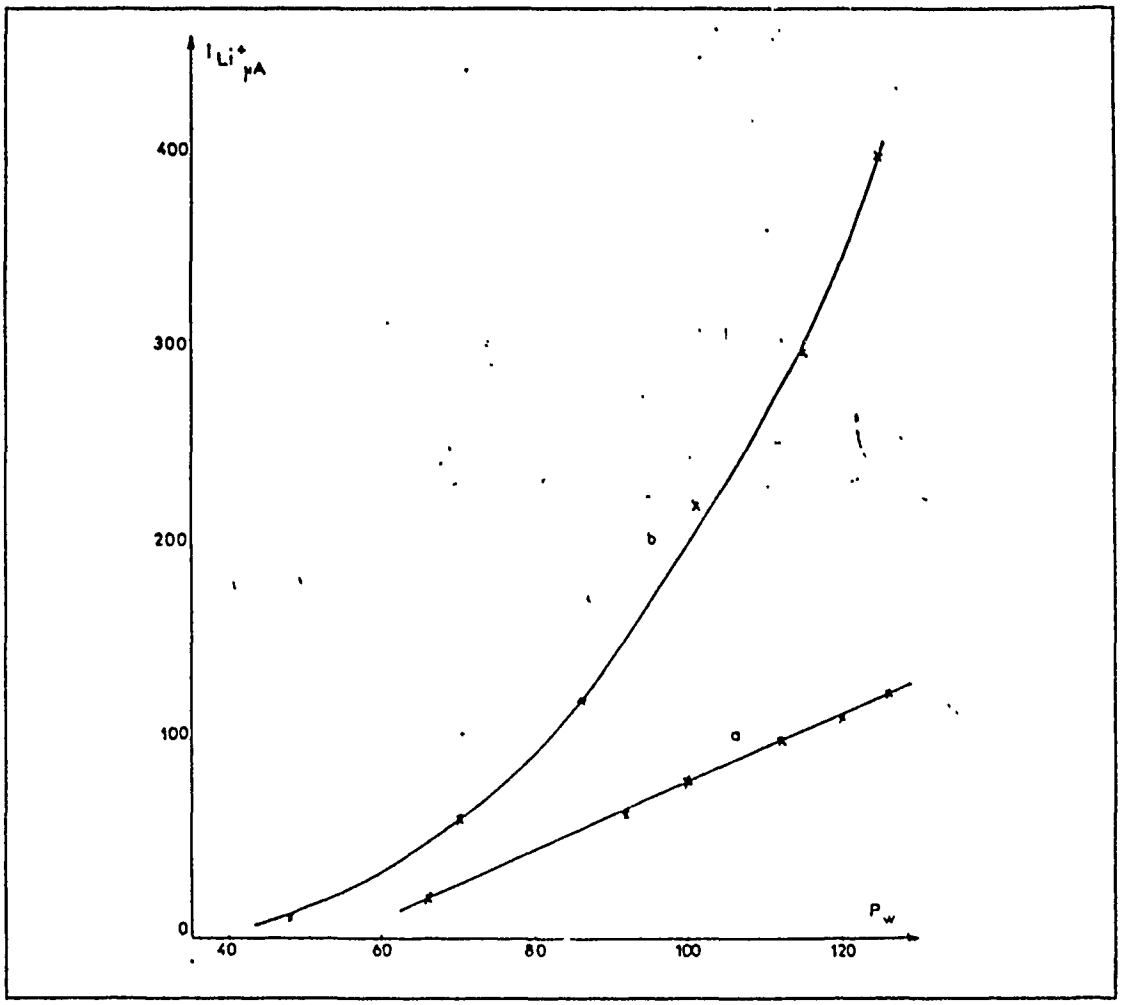

Figure 12. Li^+ ion current vs heating power.: (a)without a heat reflector (b)with a heat reflector [Ref.11]

Howard L. Daley and J. Perel developed an ion source which used direct surface ionization from oxygenated tungsten to generate lithium or sodium ion as shown in Figure 13. The theoretical efficiency of the source (described using the ratio of the number of ions desorbed to the number of ions and atoms desorbed) depends upon the difference between the work function (ϕ_w) of the surface and the ionization potential (

ϕ_i) of the species. When ϕ_w is greater than +0.5 eV, the surface ionization is very efficient. The measured efficiencies are more than 70% for both Li and Na using this type source. This is much larger than that of the capillary ion source (< 5%) developed by M. Remy and R.Haug in 1969. [Ref.12]

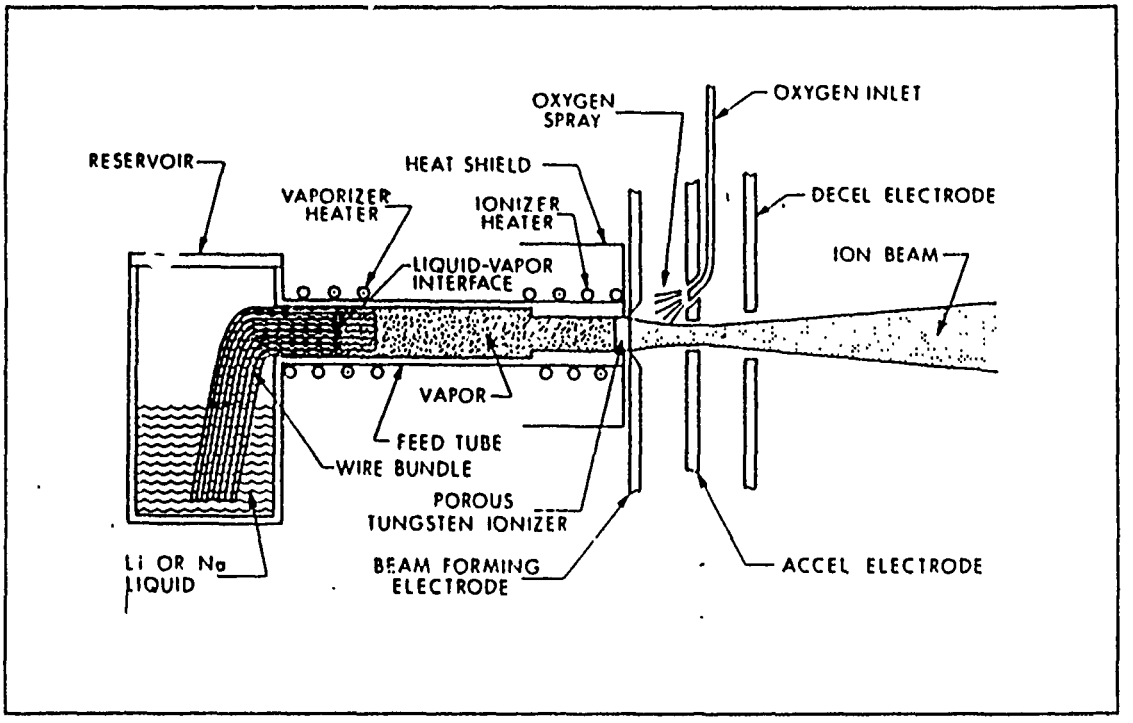

Figure 13. Schematic representation of the ion source configuration: used to generate lithium and sodium ions. [Ref.12]

R. K. Feeney, William E. Sayle used a variety of aluminosilicate sources of positive ions for atomic collision experiments. The most copious thermionic-type ion emitters have been observed to be the aluminosilicates. The emitter preparation can be expressed with the formula:

$$X_2CO_3 + nSiO_2 + Al_2O_3 \xrightarrow{heat} X_2O \cdot Al_2O_3 \cdot nSiO_2 + CO_2\uparrow \qquad (7)$$

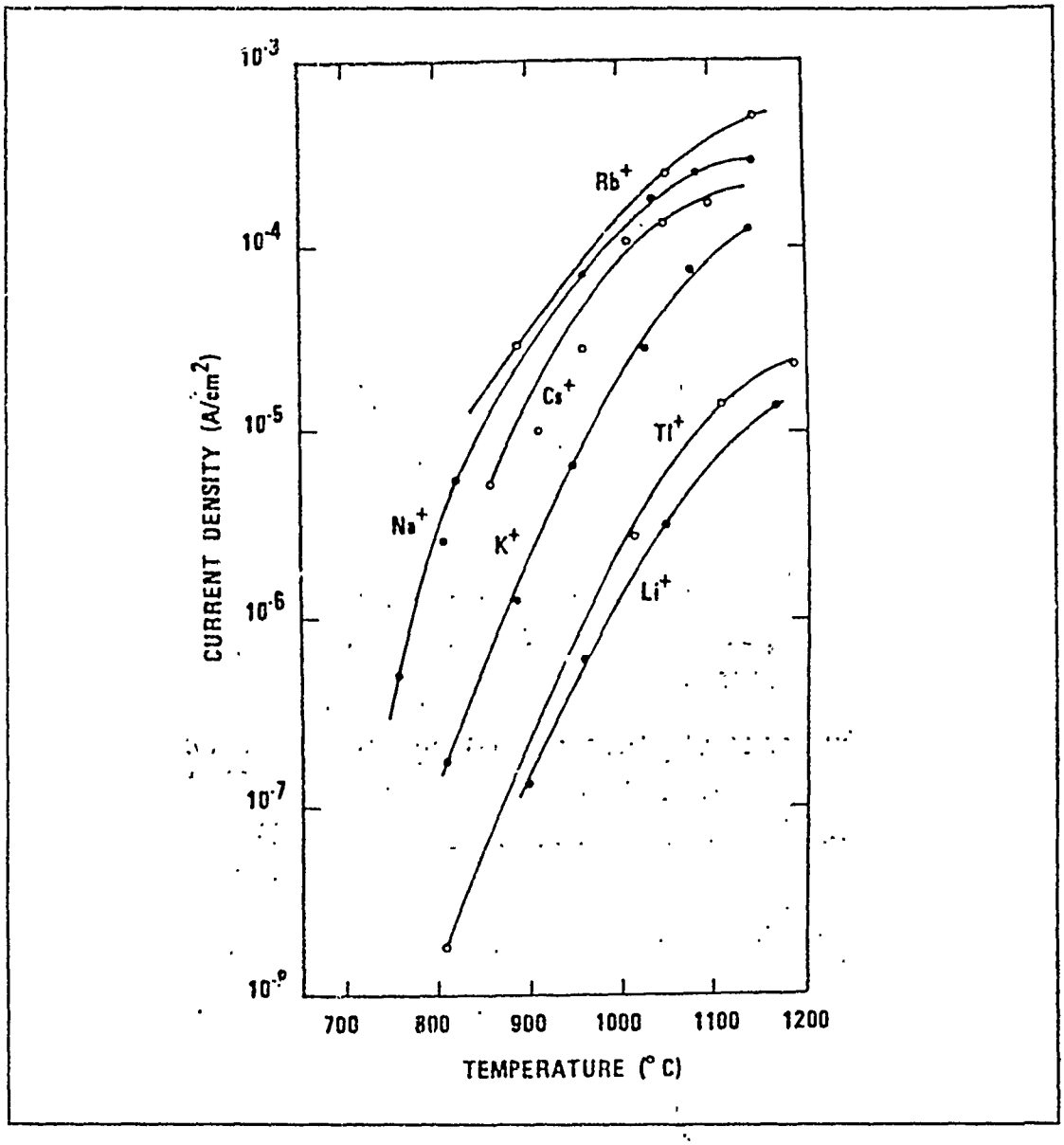

Figure 14. **Typical current densities obtainable for the various emitters:** as a function of temperature. [Ref.13]

Here X is the desired alkali elements, and n = 2 for eucryptite-like or n = 4 for spodumene-like materials, respectively. Figure 14 shows the typical total current densities obtained from the six emitters as a function of temperature for an extraction electric

field of 500 V / cm. This shows that the various aluminosilicate-type ion emitters did not give equal emission currents for the same conditions. Emitters producing collimated beams of Li^+, Na^+, K^+, and Tl^+ ions operated for about one month. The failure of a filament can terminate the emission earlier than original lifetime. [Ref.13]

4. Applications of the Spectra-Mat. Design

In certain applications the linear arrangement of ion source and charge exchange chamber in standard charge exchange sources for neutral atomic beams leads to undesirable stray light. In 1980, to avoid this problem S. Kita developed a new design using the lithium ion source developed by Heinz and Reaves. They used a commercially available version (Spectra-Mat., Inc., California). In order to prolong its lifetime the emitter surface of 15 mm diameter was masked by a cover which had an opening of 3 mm diameter, made of 0.1 mm tantalum sheet. [Ref.14]

In 1981, G. Conforti and F. Del Giallo developed a low energy (25 - 500 ev) alkali ion gun for use in collision experiments using the same lithium ion source. It fulfilled their requirements: (a) well defined beam geometry; (b) ions emitted in the ground state; (c) ion beam energy spread of a few eV. [Ref.15]

In 1988, D. M.Thomas and W. P. West used a lithium ion emitter for plasma diagnostics. For their diagnostic systems, the available neutral current was very high (1 - 2 mA). Because of emittance requirements they employed lithium ion sources based on the thermoemissive glass β-eucryptite. They enlarged the emitter area to get more than 15 mA of Li^+ emission. With 15 cm^2 of emitter area, they could get the emission current of 20 mA. Figure 15 shows the sketch of the prototype lithium ion source used in this experiment. [Ref.16]

These applications illustrate the wide range of applications for which this lithium ion source design has been used. The work designated next is intended to extend these applications in space.

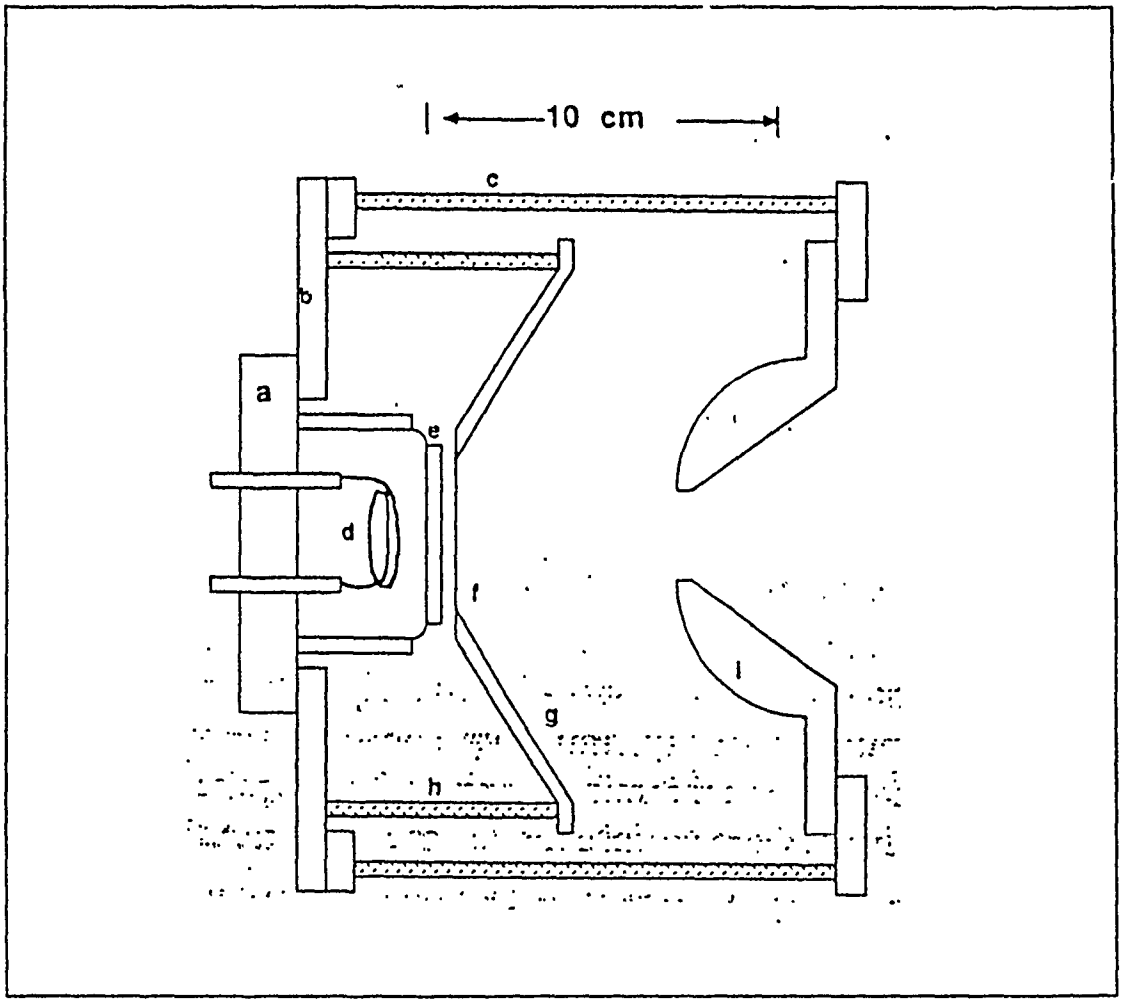

Figure 15. **Sketch of the prototype lithium ion source:** (a)source flange (b)gun flange (c)alumina insulator (d)heater filament (e)2-in. molybdenum disk with emissive coating (f)tungsten grid (g)cathode (h)cathode insulating support (i)anode. [Ref.16]

II. EXPERIMENTAL EQUIPMENT

The equipment can be divided into four main components as follows:

- Vacuum chamber
- Power supplies for the source heater
- Measurement instrumentation
- Vacuum system

A. VACUUM CHAMBER

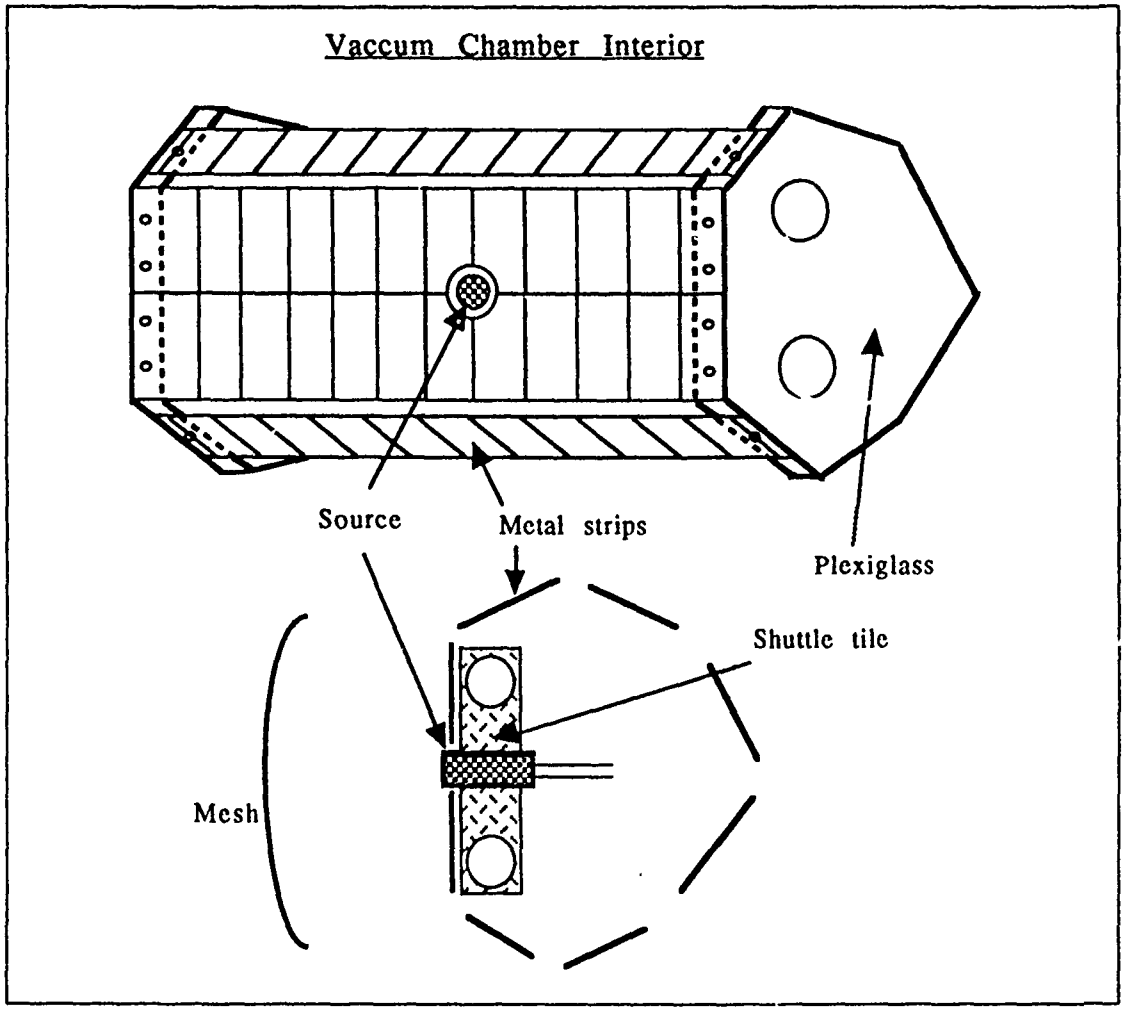

Figure 16. Vacuum chamber interior

Figure 16 is a diagram of the chamber system interior. The Lithium ion source, metal (stainless steel) strips, and the copper mesh were mounted inside the chamber.

The lithium ion source was purchased from Spectra Mat., Inc.. This source was designed originally by O. Heinz and R. T. Reaves in 1968. Spectra Mat., Inc. manufactures them commercially for scientific applications. We needed to mount the lithium source with good thermal and electrical isolation. The material used is space shuttle tile (see Appendix). The source is connected to the heater power supply through the high current feedthrough.

For later experiments, eight metal strips are mounted on plexiglass end plates of the shape of semi-cylinder. The strips are to simulate the surfaces on a satellite, and can be biased independently. The copper mesh is mounted just inside of bell jar and takes the role of plasma sheath (ground to the system) in space.

B. ELECTRONICS

We used two kinds of power supply for heating the source. One is HP 6030A DC power supply. At 100 V AC input it's output maximum was 800 W (170 V, 17 A), but we needed less than 20 W to heat the small 1/4 inch diameter source. During the experiment we found that there was some current leakage through the power supply to ground, so we changed to an AC power supply. This utilized a VARIAC and transformer. The transformer gave an impedance to ground of greater than 100 MΩ. A Keithly 230 programmable DC voltage source and Lambda DC power supply were also used to bias the source, metal strips, and metal mesh.

C. MEASURING EQUIPMENT

Two Varian Type 0531 thermocouples were used to measure the pressure in the rough vacuum range and Varian 880RS ionization guage was used to measure the high vacuum pressures.

Two Keithley 195A, 196A digital multimeter and Fluke 75, 85 multimeters were used to measure the source to mesh current, source to metal strip current and power of AC power supply respectively.

Temperatures were measured with a Leeds & Northrup optical pyrometer. Secondary measurements with a Pt/Pt Rd thermocouple (Type S) were less useful due to poor thermal coupling from thermocouple to source.

D. VACUUM SYSTEM

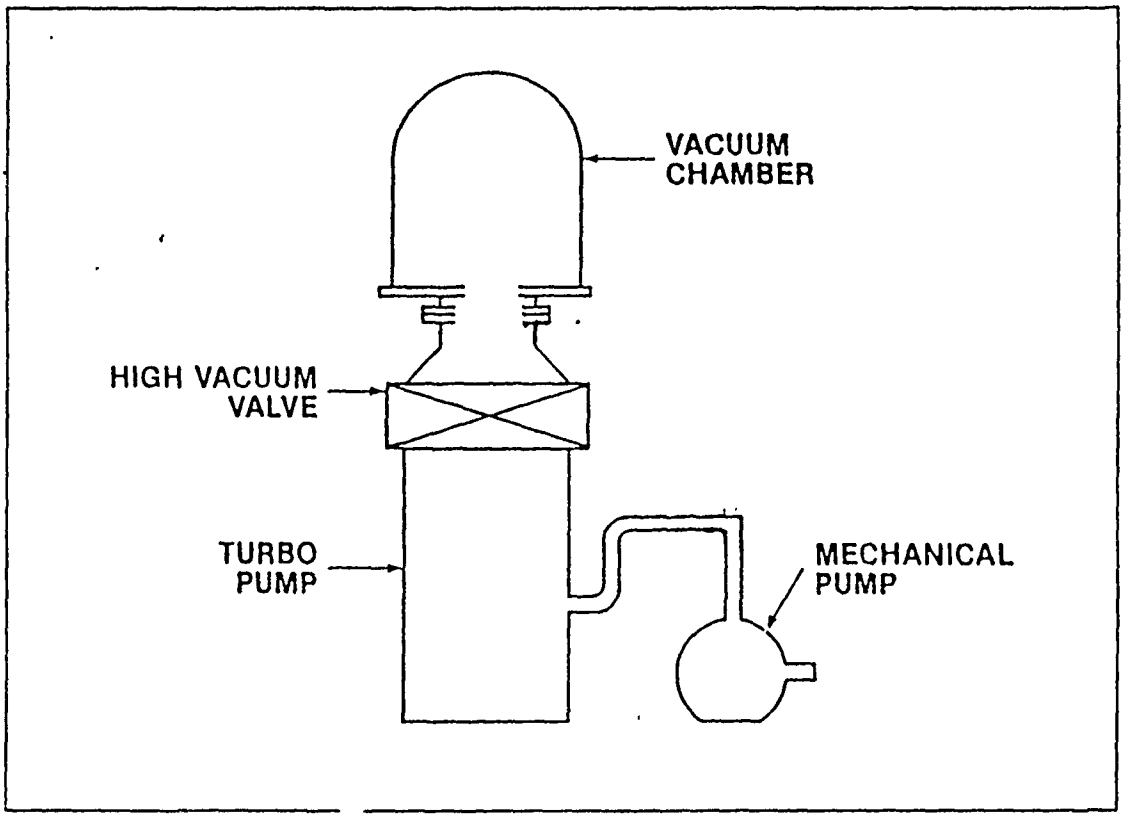

Figure 17. Sketch of Varian vacuum system

Fig 17 shows the major parts of the Varian System. This vacuum system consists of two pumps. A Rotary Vane Oil-Sealed Mechanical Pump is used for rough pumping; pressure range 760 torr to 10^{-3} torr. A Turbo-V 1000 pump is used for a high vacuum pumping; pressure range 10^{-3} to 10^{-8} torr. For this experimental system the minimum pressure requirement was about 10^{-6} torr. The pressure tended to increase when the source was heated, apparently due to outgassing from the source.

The operating procedure for this system is very important. In order to begin this experiment, the Bell Jar should be evacuated to the order of 10^{-6} torr. It usually takes several hours to reach the desired pressure range of vacuum chamber and up to 24 hours pumping to assure complete outgassing. The procedure for operating the vacuum system is as follows;

1. Turn on the cooling water and open the nitrogen gas tank valve (Nitrogen bottle pressure is set to 2.0 - 5.0 psi as the regulated pressure).
2. Place switch marked "Turbo Pump" to "Off" position.
3. Switch on power to turbo controller and ionization gauge.
4. Push "start" on controller. Mechanical pump should start, turbo pump should not. Let system pump down to 100 milli torr as indicated by TC2 gauge on ionization gauge pannel.
5. With controller in "Low speed" (i.e., Low speed button depressed) switch "Turbo pump" switch to "On" when 100 milli torr reached.
6. "Acceleration" and "Leak" indicators will light. Both should go out and "Normal" indicator will light within 5 minutes.
7. Switch on ionization gauge to read pressure.

When the source has been exposed to atmosphere, allow vacuum system to pump down at least overnight before attempting to heat the source.

III. EXPERIMENTAL PROCEDURE AND RESULTS

A. INVESTIGATION OF LITHIUM ION SOURCE

The size of the source we used in this experiment is diameter of emitting surface 0.25 inch, area 0.317 cm^2, which is smaller than the original design used by O. Heinz and R. T. Reaves (0.6 inch diameter). To use this source in spacecraft charge control, we needed to investigate the source characteristics. The primary concerns were available currents, power requirements, and how effectively it acts to cancel differential charging.

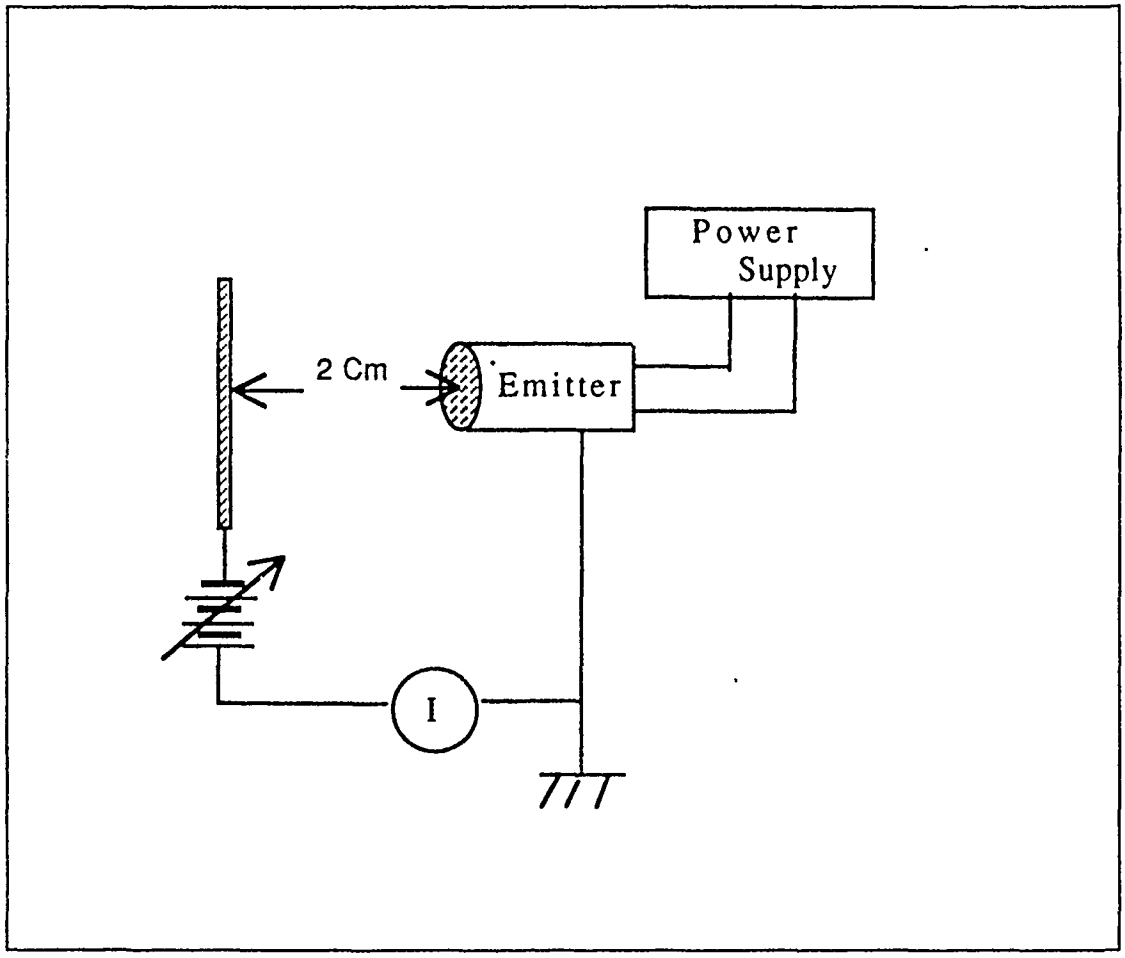

Figure 18. Diagram for measuring total current

1. Current Available

In order to determine the total emission current available as a function of input power, we constructed the circuit shown in Figure 18. Finally the grid was grounded, and the source was biased with respect to ground. Unfortunately there was some current leakage through the power supply to ground. The grounding scheme was revised, and the source was grounded. To do this experiment we set the power, and measured current by increasing the negative bias to the grid.

Figure 19 shows the plot of I vs V at three different power levels (11, 13, 15 W). The temperatures are approximately 960 $^{\circ}C$, 1000 $^{\circ}C$, and 1050 $^{\circ}C$ respectively. As shown by equation (3), the emitting current should be proportional to $V^{3/2}$. At 15 W, the slope of logI vs logV plot is 1.6, which is slightly larger than 3/2. At 11 W power, the slope is approximately 1.4. Therefore, these results roughly satisfy the Child-Langmuir law.

Theoretical calculation of space-charge limited current in the case of voltage 100V, surface area 0.317 cm^2 and distance 2 cm is 5.18 μA from equation (3). We measured 4.65 μA at 15 W, and bias voltage 100 V. These results indicate rough agreement with space-charge limited flow.

We set a bias of -100 V on the grid and measured the emission current as a function of the heater power. Figure 20 shows the total emission current as function of heater power (or temperature). Although the value of current is smaller the shape of the curve is similar to the results from the 0.6 inch diameter source shown in Figure 10. As heater power (surface temperature) increases the current approaches the space charge limited current. At heater power 18W (temperature 1130 $^{\circ}C$) the emission current was 5.8 μA which is slightly higher than the estimated for space charge limited current.

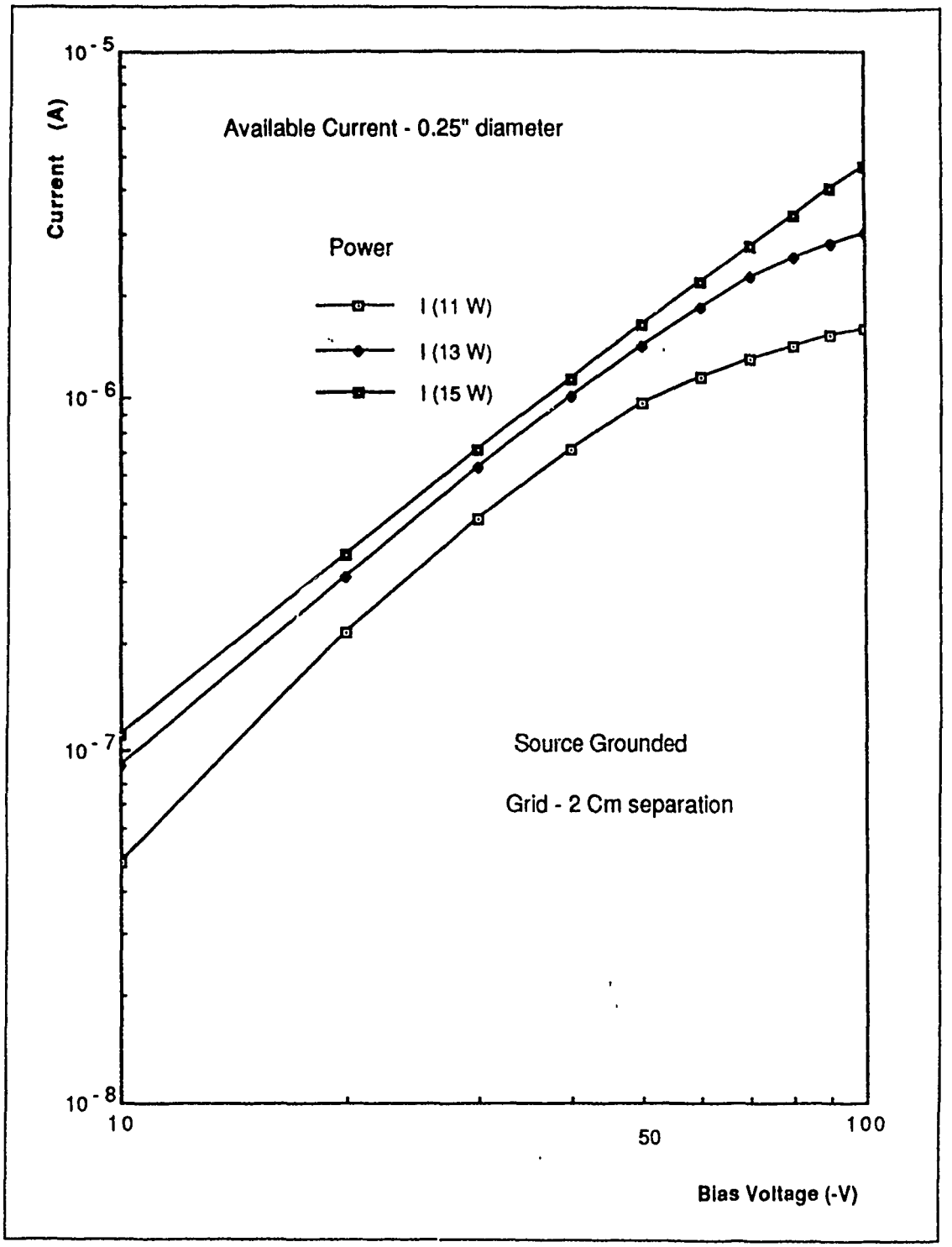

Figure 19. Emitting current as function of bias voltage to grid (negative).

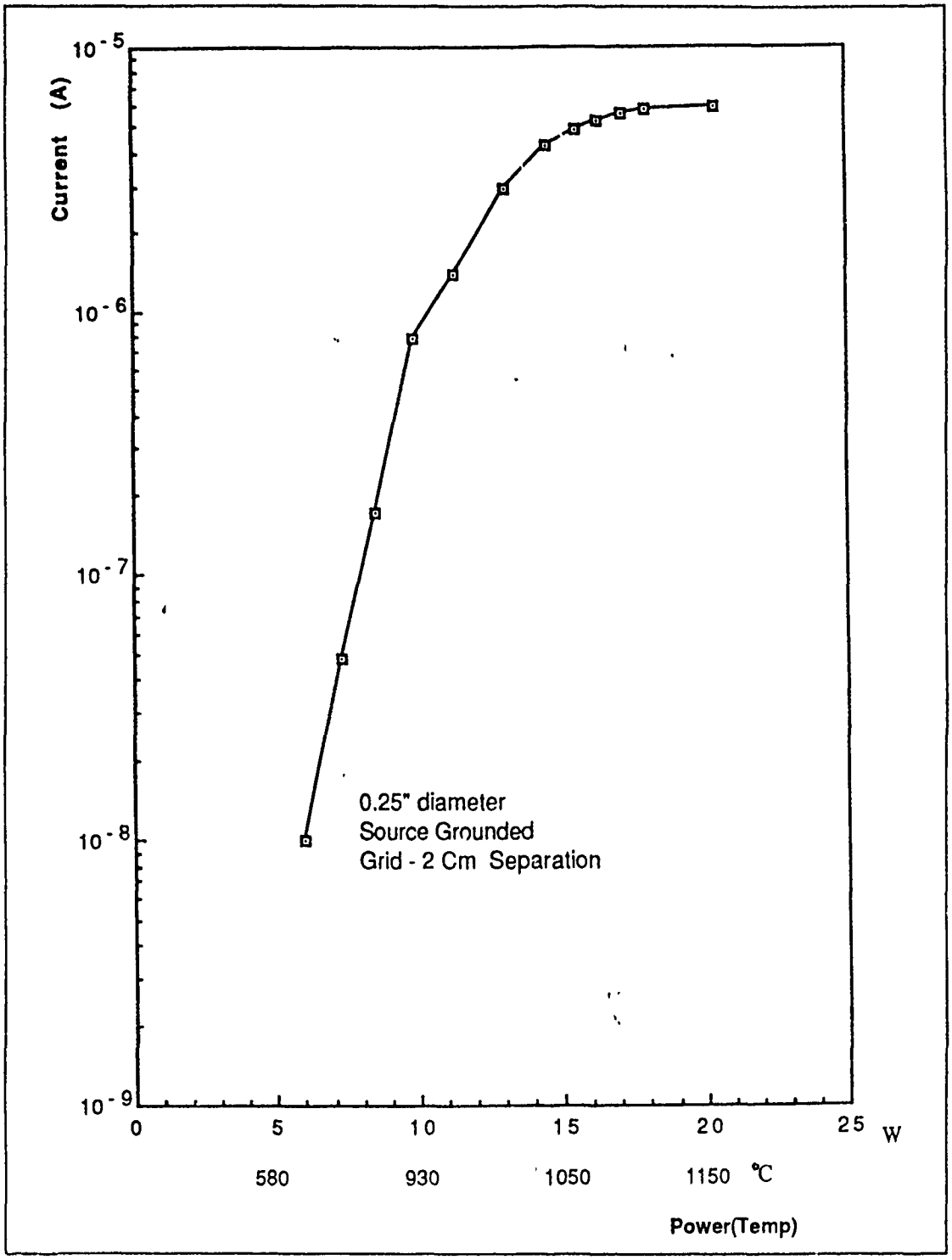

Figure 20. Total emission current as function of power (Temperature).

2. Power versus Temperature

For this experiment we connected just the power supply to the source heater and measured the temperature with a thermocouple attached to the body of the source and with the optical pyrometer (> 750°C).

Figure 21 shows the surface temperature as a function of applied power. The

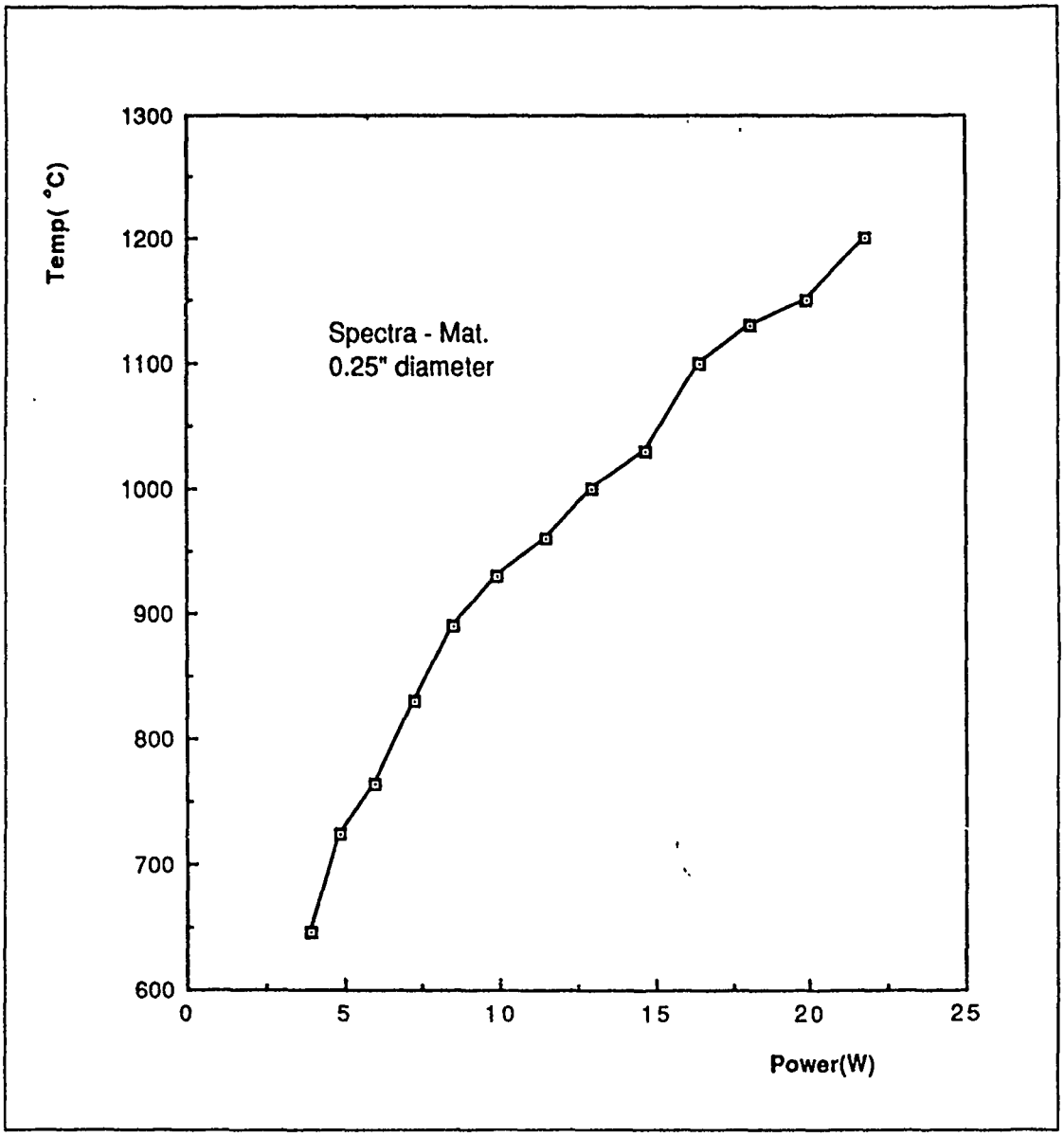

Figure 21. Source temperature as function of heater power.

temperature of the emitting surface (optical pyrometer) and the temperature of body surface (digital pyrometer) were about the same. As we can see on Figure 21, the temperature increased rapidly at very low power and increased slowly at higher power. With these data, we could estimate the temperature without using the pyrometer.

3. Temp versus Time

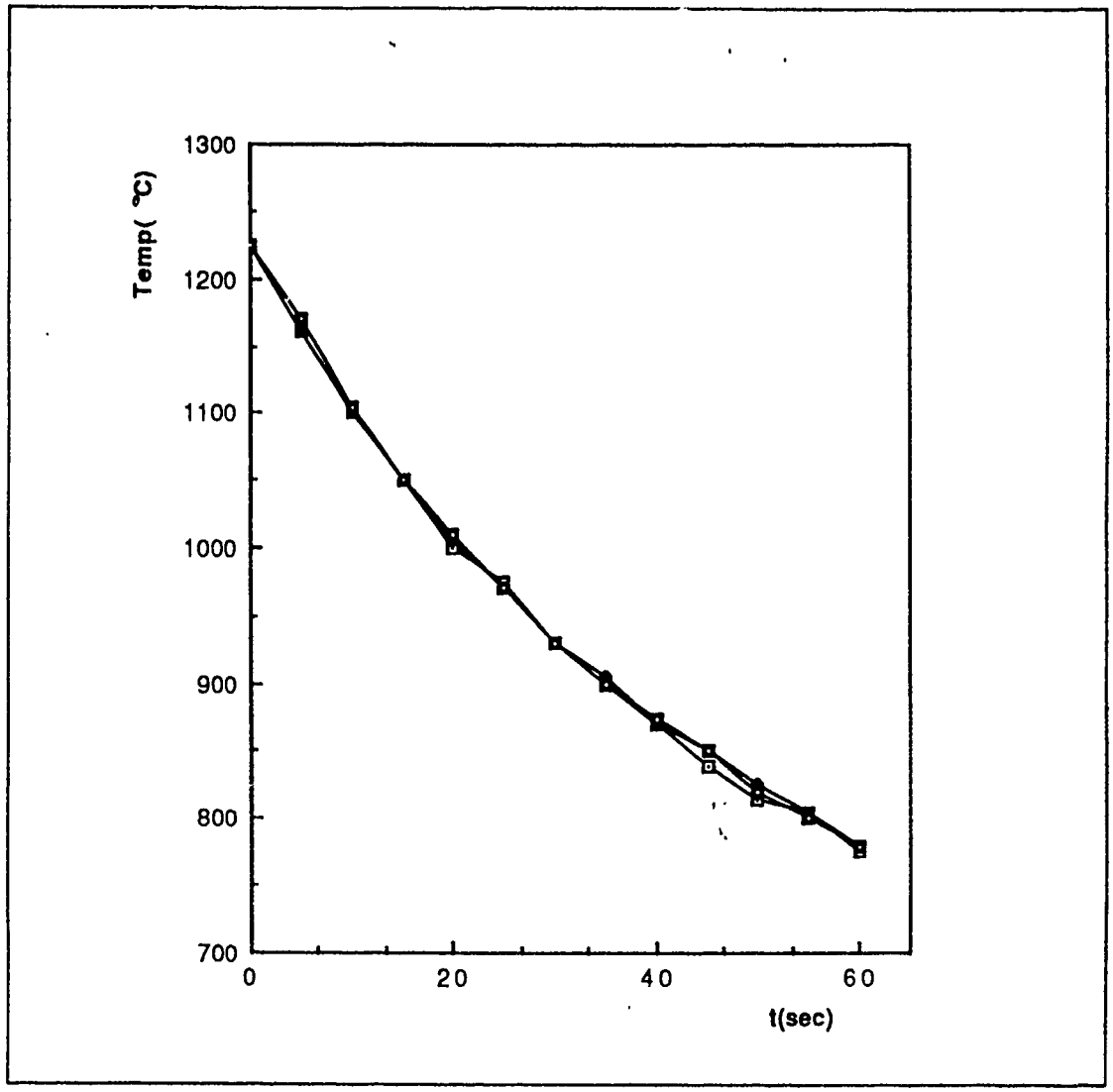

Figure 22. Measuring of temperature as function of time.

A basic question about the lithium source is how to minimize the power needed to operate the source. As a final experiment, we considered the temperature as a function of time when the source is switched off. We checked the temperature with the optical pyrometer, and needed two persons to check the time and measure the temperature. The time zero is just before the power supply is turned off. We set the power to 24W (1224 °C). The subsequent decrease in temperature is due to the radiation of heat and thermal conduction, theoretically.

As shown on Figure 22, temperature decreases with a 1 - 2 minute time constant. If we assume exponential decay (e.g. conductive heat loss), we get an equation for the curve; Temp.(°C) = 1185 × exp(-t/133.8). If we assume the losses are radiative ($dQ/dt \propto T^4$), we can also fit the data quite closely ($dT/dt = -5.1 \times 10^{-12} T^4$). The data are taken over too small a temperature range to give a truely unique answer. If we compare input power (24 W) to $Area \times \sigma_B T$ 1224 °C, and using 0.317 cm^2 we get 9 W. This suggests the two mechanisms both contribute.

B. SIMULATION OF A POSITIVELY CHARGED SPACECRAFT

To do the simulation of spacecraft charge control, we arranged the chamber as shown in Figure 16. The copper mesh simulates "space", the metal strips around the source simulate the conducting spacecraft surface.

For the initial tests, all the metal strips were connected to the body of source, and the source was grounded to the chamber base plate. The screen mesh was biased negative with respect to the source. Schematically, this arrangement is the same as in Figure 18, except the distance from source to mesh is 15 cm. The current from the source to the mesh was measured as a function of bias voltage and heater power (temperature). The flowing current was very small (0.20 μA at 23W, 1180 °C) compared to the current measured with a grid of d = 2 cm. With this level of emission current, discharging a

positively charged spacecraft would be very difficult. The normal requirement for use in space is 10 μA. This inspired us change to the setup.

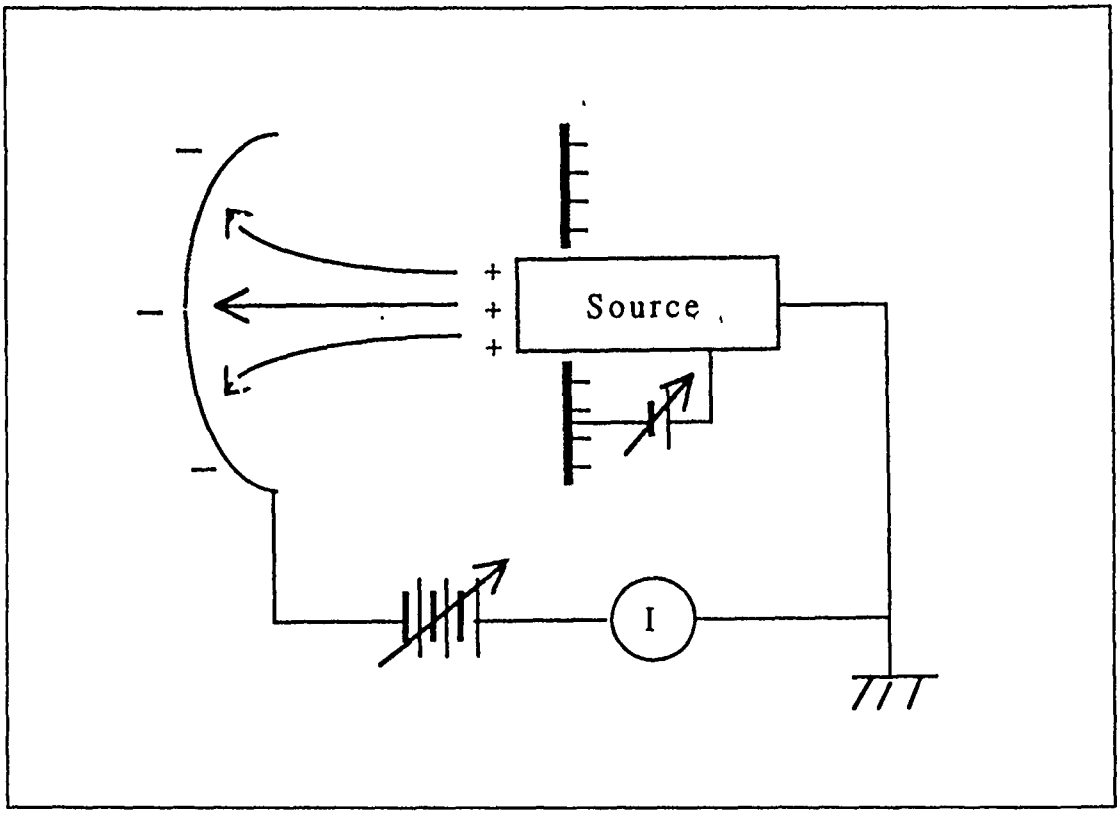

Figure 23. Diagram for simulation of a positively charged spacecraft.

We electrically disconnected the two metal strips adjacent to the source and biased the metal strips a few volts negative with respect to the source. This circuit produces an electrostatic lens, with a funnel shaped equipotential line, so accelerates the emitted lithium ions. Figure 23 shows the diagram for biasing the adjacent metal strips negative with respect to source. Conversely, a positive bias to metal strips reduced the current, just as a grid in a vacuum tube behaves. With the adjacent metal strips biased -4.06V (using a battery) we could get a much larger emission current (1.05 μA at 23 W heater power). This current is still low for our eventual goal.

Increasing the bias voltage on the metal strips increased the emission current. To increase the bias voltage we used another DC power supply (LAMBDA) which can supply up to 10 V.

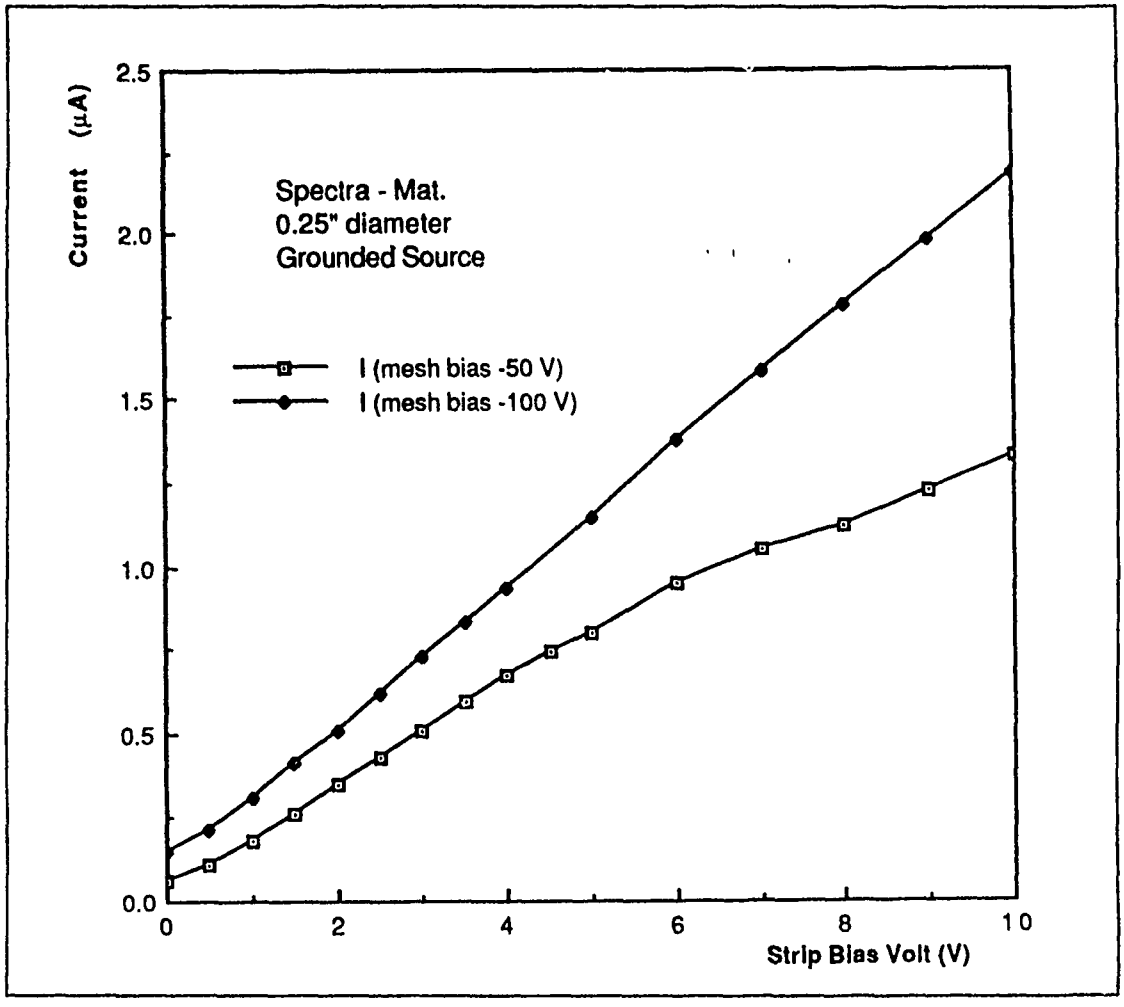

Figure 24. Emission current as function of bias voltage negative to metal strips with respect to source.

Figure 24 shows the emission current as a function of bias voltage to the metal strips. The emission current increased almost linearly with increasing bias voltage. At bias voltage to mesh -50 V, -100 V and bias voltage to metal strips -10V, the emission currents were 1.05 μA and 2.20 μA respectively (Temp. = 1170°C).

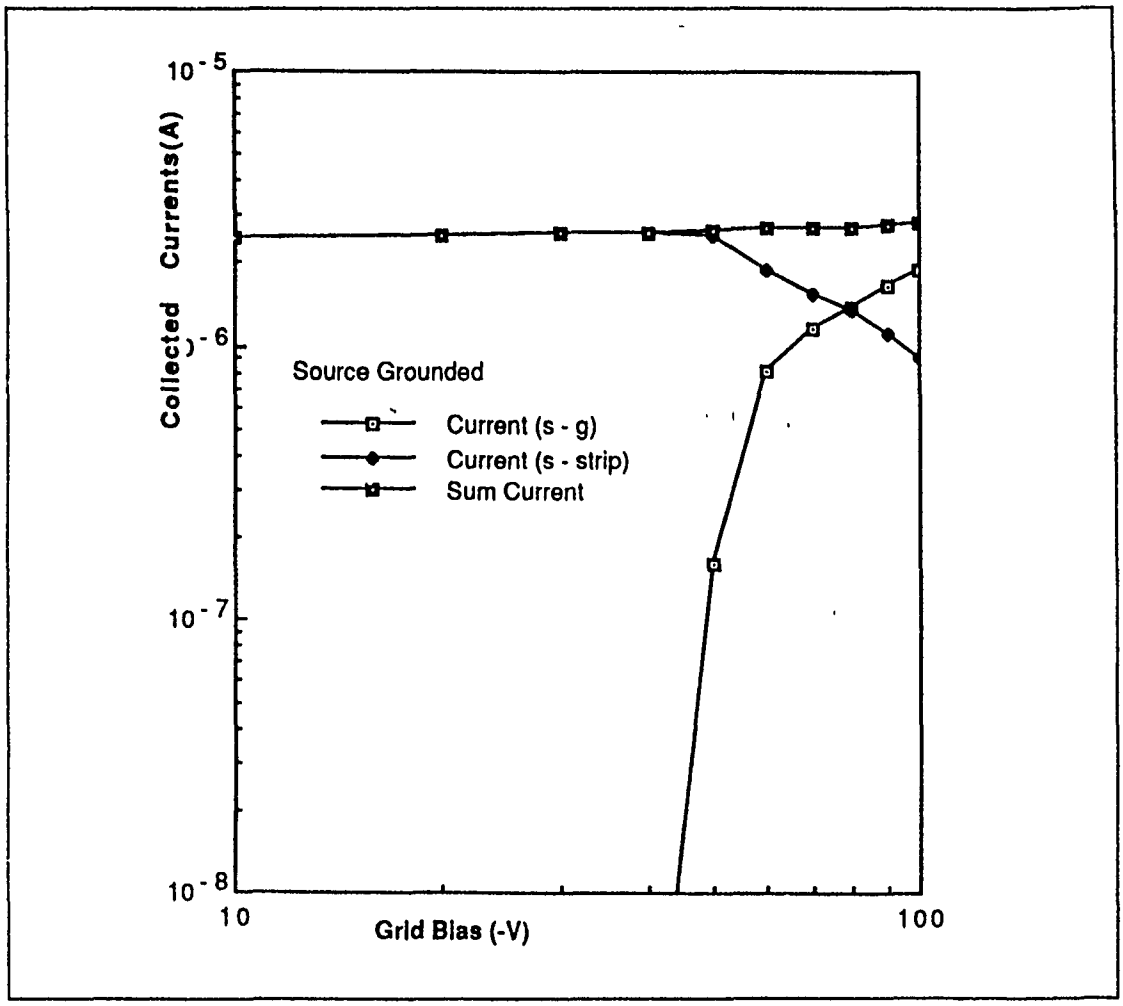

Figure 25. Emission current as function of bias voltage to mesh: w.r.t. source, at power 21 W, Temp. 1148°C, bias -10 V to strips.

Figure 25 shows the emission current as function of mesh bias voltage with source grounded and strips biased -10 V w.r.t. source. Note that the current sum (s - grid, s-strips) remains nearly constant of a value of 2.4 μA. With this 2.0 μA emission current we began to approach our goal.

A common problem in experiments like this is chamber effects. In particular, we were worried about currents flowing to the base plate. To study these effects, we floated

the source with respect to chamber ground. We grounded the mesh, biased the source positive with respect to the mesh and biased the source positive with respect to adjacent metal strips. We measured both currents from source to mesh and also to the adjacent two metal strips. Figure 26 shows the diagram for this experiment. For this experiment we used an AC heater power supply because there was some current leakage through the HP 6030 DC power supply to ground.

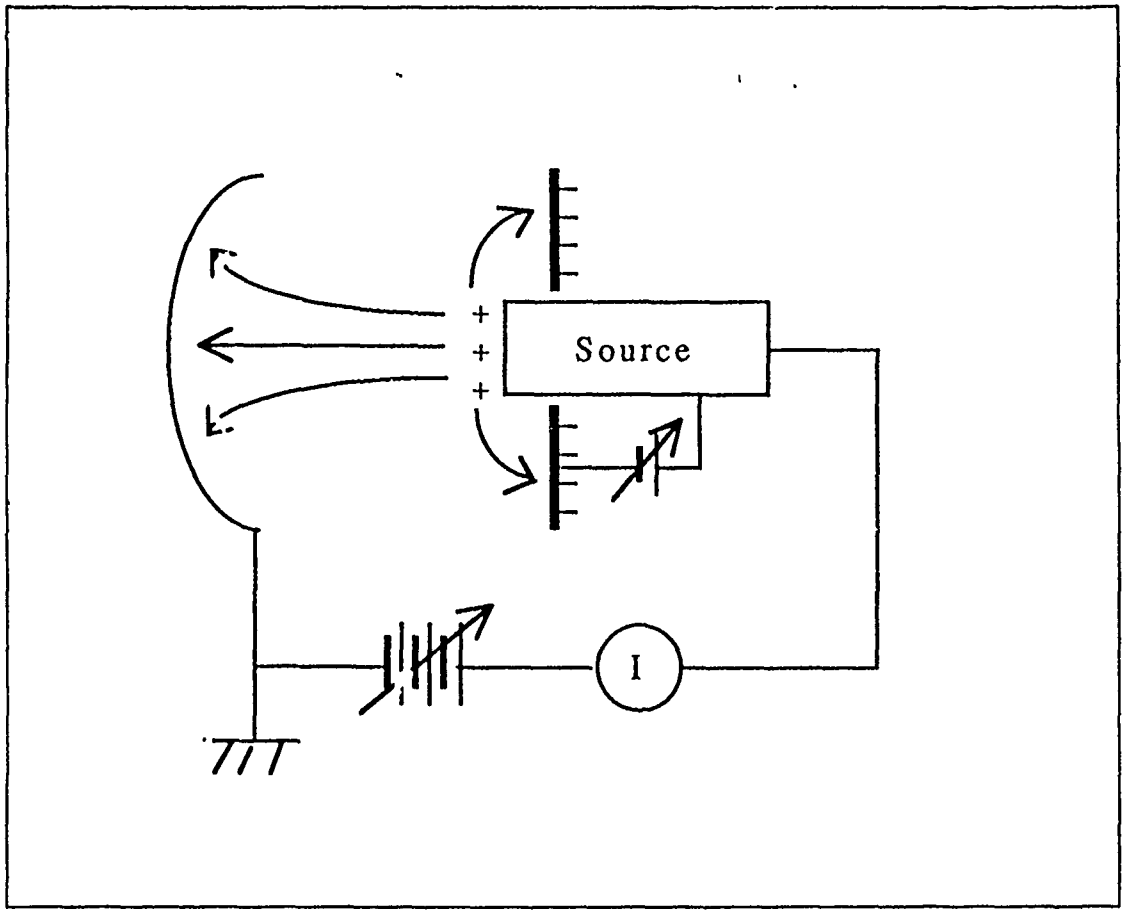

Figure 26. Diagram for checking the effect due to the geometry of chamber.

The plot of emission current versus the bias voltage between the source and metal strips remains almost linear as in Figure 27. This is similar to the case of grounding the source as shown in Figure 24.

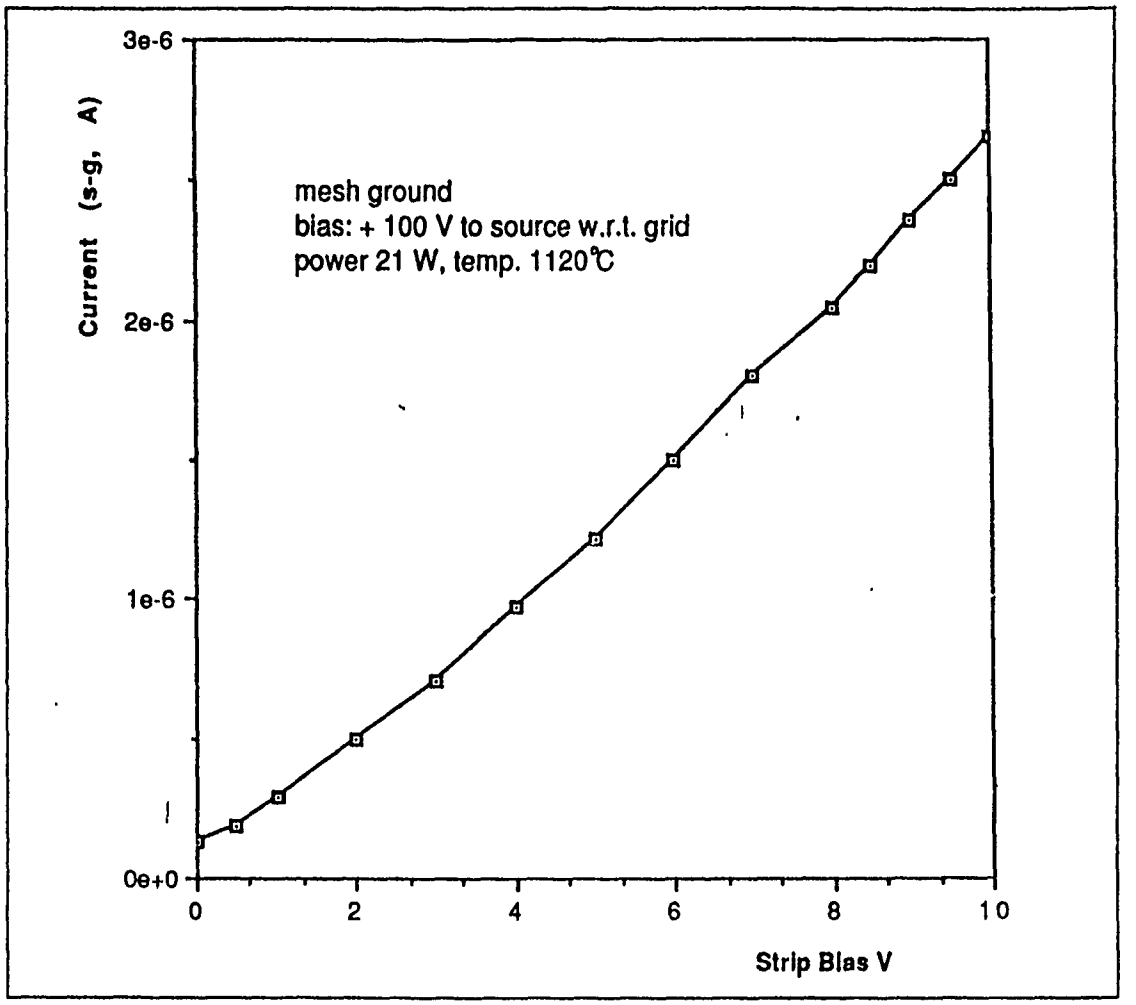

Figure 27. Emission current as function of bias voltage to strip: negative w.r.t. the source, mesh grounded.

The emission current versus heater power plot is similar to previous results, also, as shown in Figure 28. The source was biased + 100 V w.r.t. mesh, and the metal strips were set to -10 V w.r.t. the source. At heater power 21 W (1120 °C) 2.65 μA was measured. This is a little larger than the current obtained by grounding the source (2.2 μA at 1170 °C). Note, however, that Figure 20 shows current collection to a nearby grid, as opposed to the large screen mesh.

The plot of logI versus logV (bias voltage to source with respect to mesh) is shown in Figure 29. The bias voltage to the adjacent metal strips was held at 10 V, and power was set to 21 W. We measured the currents both source to grid and source to metal strips. The slopes of the curves are very similar to those shown in Figure 25. This indicates that there are not any major chamber effects in our results. The slope of the current from source to grid versus bias voltage is about 1.8 in the 30 V to 60 V range, which is a little larger than the Clild-Langmuir Low suggests ($I \propto V^{3/2}$). At higher bias

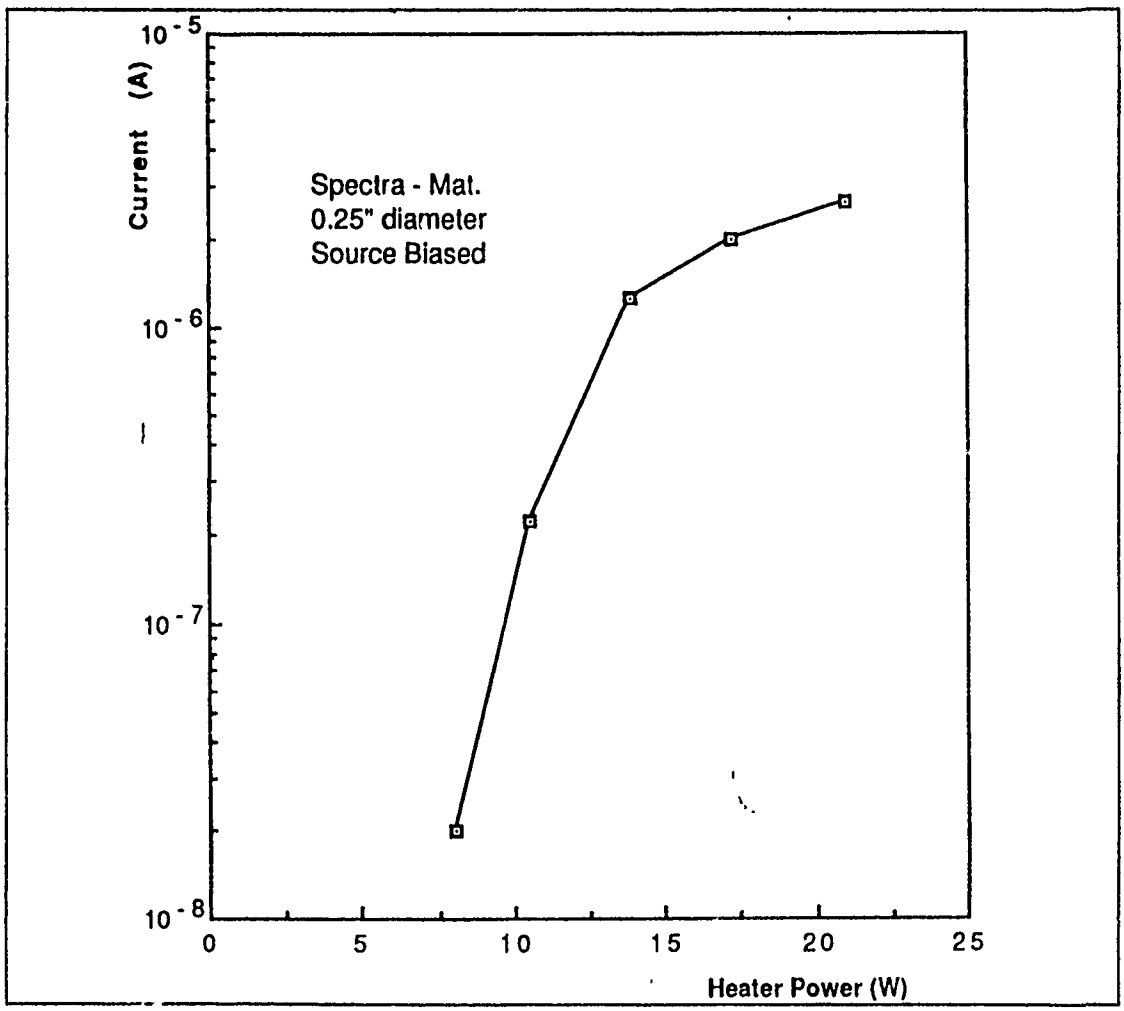

Figure 28. Emission current versus applied power: ground the mesh, bias to source + 100 V w.r.t. mesh, bias + 10 V w.r.t. metal strips.

voltages the current may be limited by ion production. Deviations from Child-Langmuir may be due to the geometry of the mesh (cylindrical) and the non ideal equipotential distribution. As the bias voltage to the outer screen is reduced, the current begins to flow to the metal strips adjacent to the source. The total current remains almost constant, dropping from 2.8 μA to 2.4 μA as the bias is decreased from 100 V to 10 V. This is a little larger than the current obtained in the case of grounding the source (see Fig. 25).

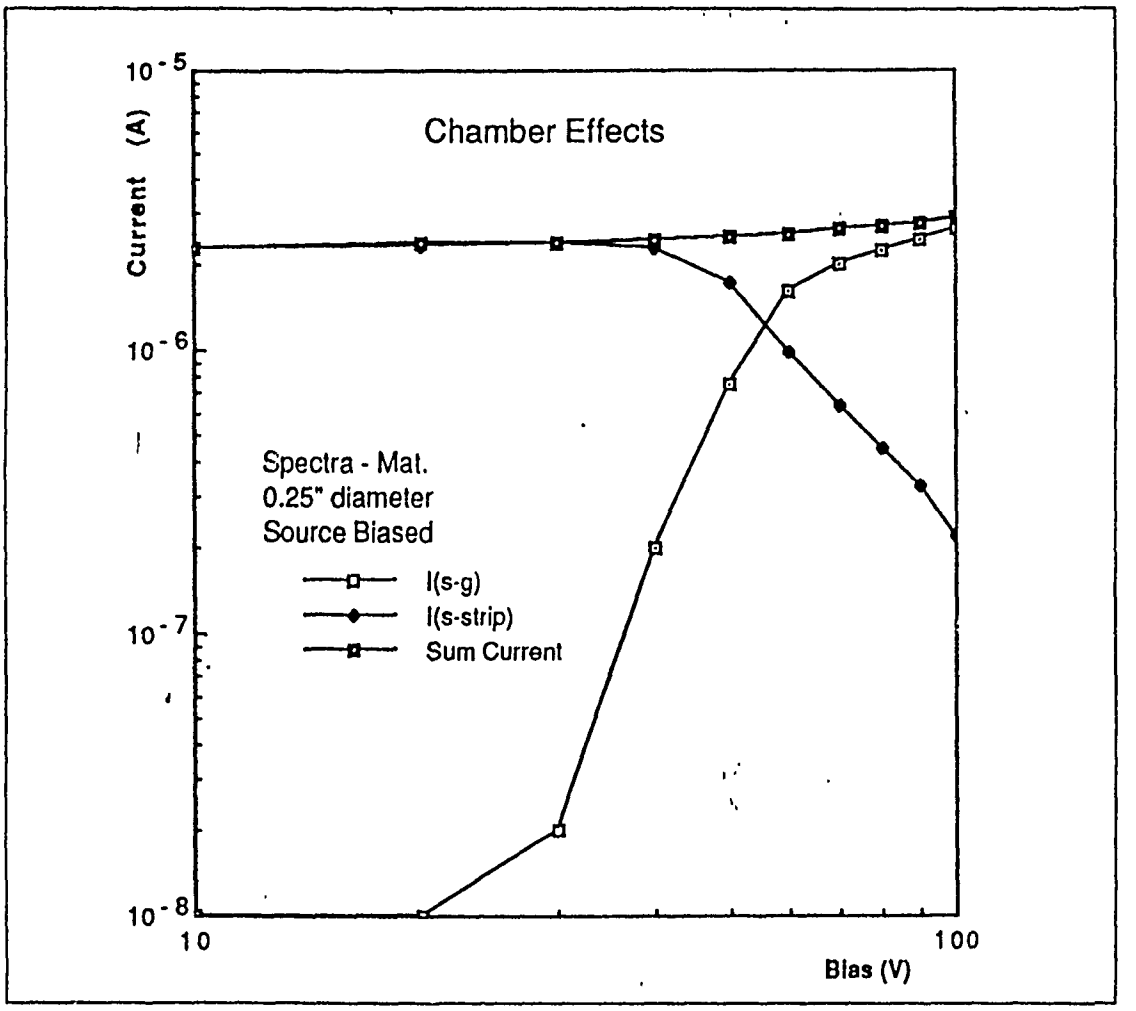

Figure 29. Emission current versus bias voltage to source w.r.t. mesh: ground the mesh, bias to source + 10 V w.r.t. metal strips, power 21 W.

C. DISCHARGE OF DIFFERENTIAL CHARGING

The second major application of a device like the lithium source is to control differential charging. To simulate the control of a differentially charged dielectric surface, we arranged the circuit as shown in Figure 30. We grounded the source and metal strips to the base plate and biased the isolated metal strips negative up to -100 V.

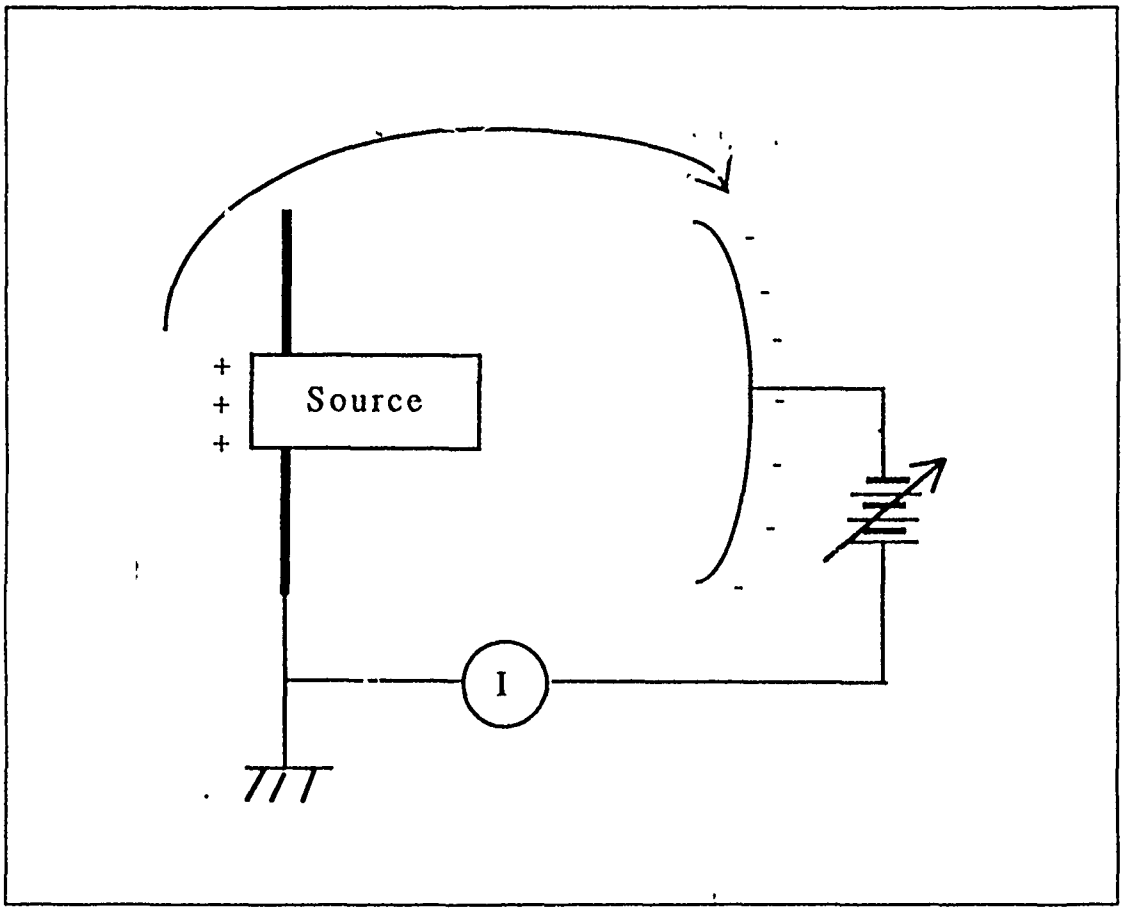

Figure 30. Diagram for control of differential charging.

The resultant current was 0.05 μA at source temperature 1200 °C. These data show us that it would be difficult to control the differential charging with the small source. We did not try using a bigger source (1.52 cm diameter) due to lack of time.

D. LIFETIME TEST

We used two sources for our complete experiments. Both were tested for lifetime. The first source expired after 52 hours of use. The second lasted through all subsequent experiments, and was then run to exhaustion. The circuit arrangement we used for this test is shown in Figure 22, i.e., ground the mesh, bias the source + 100V with respect to mesh, and bias the source + 10V with respect to adjacent two metal strips. Figure 31 shows the resultant current as a function of operating time.

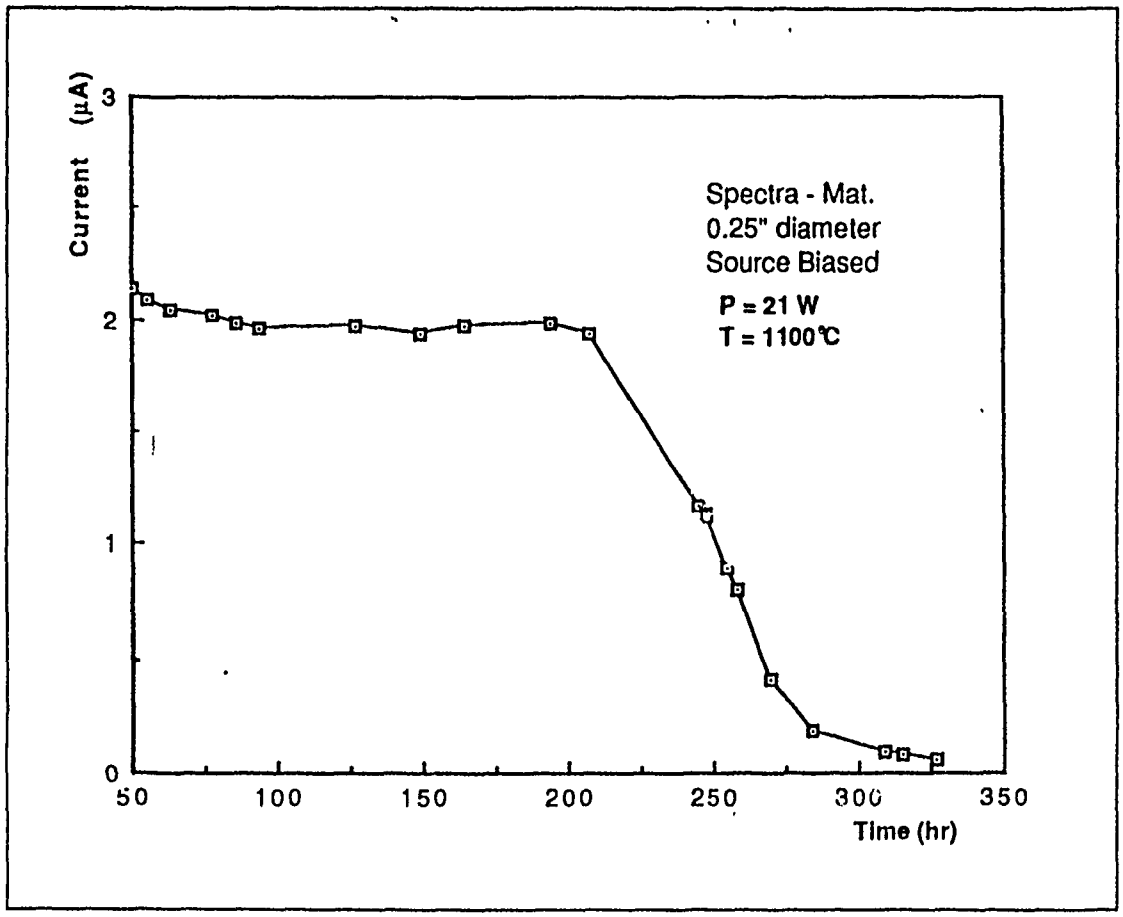

Figure 31. Emission current as function of operating Time.

Heater power and bias voltage varied for the first 40 hours, as other experiments were done. Initially, the maximum current was about 2.4 μA and the current sum (source

to mesh and source to adjacent metal strips) was almost constant ($\approx 2.7\mu A$). After 40 hours of operation, we set the power to 20W (T = 1100 °C) and the bias voltages were set to 100V, 10V respectively. About after 85 hours of operation the current from source to mesh decreased to about 2.0 μA, and the current sum also decreased to 2.4 μA. This is still good emission current for this source. The current did not vary until 200 hours of operation. After 200 hours of operation it began to decrease. At about 250 hours the current had dropped from 2.0 to 0.2 μA as seen in Figure 31. The final current was 0.1 μA.

This set of experimental data indicate that the practical lifetime for the 1/4 inch diameter source would be 200 hours. The lifetime also would depend on the operating power, i.e., the operating temperature of the emitting surface.

IV. SUMMARY AND DISCUSSION OF RESULTS

The objective of this experiment was to verify that the lithium ion source can be used for spacecraft charge control. The emission currents were measured under various condition. The properties of the 0.25 inch lithium ion source were investigated.

A. SUMMARY OF RESULTS

The lithium ion source generally behaves according to the Child-Langmuir law (see Fig.18). The slope of logI vs logV was around 1.5 at different power levels. The emission current saturated at 5.8 μA, using a heater power of 18 W. The larger source should allow up to 40 μA (see Fig.10).

Experiments were conducted with the ion source mounted in an 8 inch long by 5 inch diameter structure allowed simulation of the source mounted on a spacecraft. A copper mesh was installed on the interior of the bell jar surface, 15 cm from the source. Without a bias between the source and adjacent metal strips, the emission current was very small (0.20 μA at 23 W). With the source biased 10 V positive w.r.t. adjacent metal strips, the measured emission current was increased up to 2.20 μA at temperature 1170 $^{\circ}C$ (see Fig.23,24). This current could be significant for control of spacecraft charging.

Effects due to geometry of the chamber was tested by grounding the mesh, and floating (or biasing) the source. The resulting I - V curves were similar to results obtained with the source grounded, indicating there were not any major chamber effects. The slope of I vs V was about 1.8 at voltage range 30 to 60 V, which is a little larger than expected from the Child- Langmuir law (see Fig.19,29).

The discharging of differential charging on dielectric surface was tested by isolating the metal strips which were on the opposite side of the emitting surface and biasing these metal strips negative (see Fig.30). The emitting current to these metal strips by diffusion

was very small. We need a bigger source to check the discharging of differential charging.

The lifetime was tested for the 0.25 inch source. Emission current was initially 2.0 μA, for about 200 hours at 20 W power. Over the next 50 hours of operation the current dropped to 0.2 μA (see Fig.29).

Evaluation of the thermal characteristic of the source indicates roughly equal contributions to heat loss by thermal conduction and radiation.

B. DISCUSSION OF RESULTS

The investigation of lithium ion source using a 0.25 inch diameter of emitting surface gave us similar results to the 1.52 cm (0.6 inch) diameter source. The emitting current was smaller than obtained from the 1.52 cm source, but the shape of plot (current vs power) was almost identical to that observed using the bigger source (see Fig.10,20). Plots of current vs voltage showed us that this source satisfied the Child-Langmuir law roughly. The lifetime of the source is similar to claims for the 1.52 cm diameter source.

Discharge of positively charged spacecraft is simulated easily assuming the copper mesh is outer space which is grounded and the source is attached to the spacecraft surface (metal strips). For geosynchronous orbit, the spacecraft potential is about + 10 V in sunlight and the photoelectron current is about 10 μA. An emission current of 2-10 μA can reduce the spacecraft potential to near zero. The size of the source should be larger than the one used in this experiment, in order to increase the emission current capability up to 20 μA.

V. CONCLUSIONS

Experiments using a lithium ion source to simulate the control of spacecraft charging were successfully conducted in a small bell jar vacuum system.

The lifetime was about 200 hours. Some method is needed to increase the lifetime of the source, like the capillary ion source. The emission current available from the source varies proportionally with the emitting area of source. The 0.25 inch diameter source is marginal for anticipated flight applications.

Simulating the actual spacecraft condition in the vacuum chamber we could simulate the discharging effect of positively charged spacecraft. The emission current of 2.0 μA for a 0.25 inch diameter source gave us the strong possibility of discharging the spacecraft if we use a bigger source to get a larger current. Differential charging on the dielectric surface of spacecraft may also be controllable by using a bigger source. Experiments with experimental spacecraft using the lithium ion source is recommended in the future.

APPENDIX SPACE SHUTTLE TILE CHARACTERISTICS

When NASA's space shuttle orbiters re-enter earth's atmosphere from space, they will encounter temperatures as high as 2300 *'F*. To protect the orbiters and their passengers from such temperatures, Lockheed Missiles & Space Company has developed a high-purity silica fiber insulation that sheds heat quickly.

They manufactured in two forms; LI-900 (9 lbs per cubic foot) and LI-2200 (22 lbs per cubic foot). The basic raw material for LI-900 and LI-2200 is a short-staple, 99.7% pure amorphous silica fiber that is derived from common sand. A slurry containing fibers mixed with water is frame cast to form soft, porous blocks to which a colloidal silica binder solution is added. When dried and sintered, a rigid block of LI-900 is pro luced. Coatings of silica frit are baked on in 15 mm thickness. Tiles for high temperature (up to 2300 *'F*) use a black Class 2 reaction-cured boro-silicate glass coating (RCG). For lower temperature use at 750 - 1200 *'F* on upper surfaces, a white Class 1 silica compound is used with shining alumina oxide. The data sheet for LI-900, which used in our experiment, is attached at following pages. [Ref.17]

Lockheed Missiles & Space Co., Inc. developed LI-900 as a unique new rigid insulation material for the Space Shuttle Thermal Protection System. When protected by a black reaction cured glass (RCG) coating, LI-900 tiles attached to the underside of the space shuttle can withstand the searing heat of 100 reentry cycles without damage. The coating reradiates approximately 90 percent of the heat generated during each reentry back into deep space or the upper atmosphere. The tile insulation material absorbs the remaining energy, preventing the aluminum surface of the orbiter from exceeding 350°F.

Summarized below are the principal properties of LI-900; the values cited were obtained in connection with the Shuttle Program.

- **Low Conductivity.** LI-900 conductivity at 500°F is only 0.52 BTU-in./ft^2 -hr-°F, compared to a value of 0.30 BTU-in./ft^2-hr-°F for still air.
- **Low Density.** LI-900 has a density of only 9 lb per cubic foot.
- **Purity.** LI-900 is 99.7 percent pure SiO_2. It has no organic constituents that will outgas to contaminate parts or equipment.
- **Long Life in Cyclic Applications to 2300°F.** LI-900 does not degrade with cyclic exposure to 2300°F. It can withstand limited exposure to 2650°F.
- **Rigidity.** LI-900 can maintain shape and support light mechanical loads while providing thermal insulation.
- **Consistency of Product.** Processed to exacting specifications, all LI-900 material meets minimum strength and conductivity requirements.
- **Dimensional Stability to 2300°F.** LI-900 has an extremely low coefficient of thermal expansion (3.2×10^{-7} in./in./°F from 0 to 2000°F).
- **Unusual Thermal Shock Resistance.** Because of its low coefficient of thermal expansion, LI-900 heated to 2300°F can be immediately immersed in cold water without damage.
- **Inert.** LI-900 does not react with most fluids and substances.
- **Nonflammable.** LI-900 does not burn; the material softens above 2500°F and melts at about 3100°F.
- **Low Dielectric Constant.** The relative (to vacuum) dielectric constant for LI-900 is less than 1.15 over the temperature range to 2100°F.
- **High Diffusivity.** LI-900 contains over 90 percent voids by volume and offers minimal resistance to the passage of gases during pressure equalization.

LI-900 is a cast material with anisotropic properties. The higher mechanical properties are in the in-plane direction, whereas the high "insulation" (or lower thermal conductivity) properties are in the through-the-thickness direction.

RF characteristics and mechanical properties at room temperature and thermophysical properties over a range of temperatures are shown in Tables 1 through 3. Mechanical properties remain relatively constant up to 1600°F, where a gradual reduction in strength begins. Mechanical properties at cryogenic temperatures are generally somewhat higher than room temperature properties. The room temperature standard deviation for tensile strength, based on approximately 2,000 tests, is 5 psi in the through-the-thickness direction and 10 psi in the in-plane direction.

Table 1 REPRESENTATIVE RF CHARACTERISTICS AT 10 GHz (ROOM TEMPERATURE)

	DIELECTRIC CONSTANT	LOSS TANGENT
LI-900	1.13	0.0004
RCG Coating	4.80	0.0030

Table 2 TYPICAL LI-900 MECHANICAL PROPERTIES AT ROOM TEMPERATURE

DIRECTION	PROPERTY	VALUE (psi)
In-Plane	Tensile Strength	68
	Tensile Modulus of Elasticity	25000
	Compressive Strength	70
Through-The-Thickness	Tensile Strength	24
	Tensile Modulus of Elasticity	7000
	Compressive Strength	28

Table 3 TYPICAL LI-900 THERMOPHYSICAL PROPERTIES

MEAN TEMPERATURE (°F)	THROUGH-THE-THICKNESS THERMAL CONDUCTIVITY[1] (BTU-IN /FT^2-HR-°F) PRESSURE (ATM) 10^{-4}	10^{-3}	10^{-2}	10^{-1}	1	SPECIFIC HEAT[2] (BTU/LB-°F)	THERMAL EXPANSION[3] ($\Delta L/L_0$)
-250	0 08	0 09	0 18	0 26	0 28	0 070	$-0\,5 \times 10^{-4}$
-150	0 07	0 10	0 20	0 28	0 30	0 105	$-0\,5 \times 10^{-4}$
0	0 09	0 12	0 22	0 30	0 33	0 150	$-0\,1 \times 10^{-4}$
250	0 11	0 15	0 27	0 38	0 41	0 210	$+0\,4 \times 10^{-4}$
500	0 15	0 20	0 33	0 48	0 52	0 252	$1\,4 \times 10^{-4}$
750	0 21	0 26	0 39	0 59	0 64	0 275	$2\,2 \times 10^{-4}$
1000	0 28	0 33	0 47	0 72	0 79	0 288	$3\,4 \times 10^{-4}$
1250	0 37	0 42	0 59	0 87	0 94	0 296	$4\,4 \times 10^{-4}$
1500	0 50	0 55	0 74	1 05	1 13	0 300	$5\,0 \times 10^{-4}$
1700	0 64	0 70	0 88	1 22	1 31	0 302	$5\,6 \times 10^{-4}$
2000	0 88	0 94	1 13	1 52	1 63	0 303	$6\,2 \times 10^{-4}$
2300	1.16	1 23	1 39	1 06	2 00	0 303	–

NOTE TOLERANCES ARE·
1. THERMAL CONDUCTIVITY ± 18% OR ±0 04, WHICHEVER IS GREATER
2. SPECIFIC HEAT ± 10% OR ±0 02, WHICHEVER IS GREATER
3. THERMAL EXPANSION ± 12% OR ±0 3 X 10^{-4} WHICHEVER IS GREATER

For the Space Shuttle , LI-900 is provided with hard borosilicate glass coatings on the outer surface. These coatings increase material durability and resist rain impingement, fluid contamination, sand and dust impingement, fungus and ozone exposure, salt spray exposure, and handling damage. The coatings also control optical properties such as emittance and solar absorptance. Typical optical, thermophysical, and mechanical properties for the coatings currently in use on the shuttle orbiter tiles are given in Tables 4 through 6. Class 1 (white) coating is used on the upper surfaces of the orbiter, while RCG (black) coating is used on he bottom surfaces.

Table 4 TYPICAL COATING OPTICAL PROPERTIES

COATING	PROPERTY	VALUE	TEMPERATURE RANGE (°F)
Class 1 (to 1200°F)	ϵ_{TH}	0.82	-170 to 75
		0.74	750
		0.70	1000
		0 66	1200
	α_S/ϵ_{TH}	0 35	-170 to 135
RCG (to 2300°F)	ϵ_{TH}	0.8	-170 to 2300
	α_S/ϵ_{TH}	0.9 to 1.1	-170 to 250

NOTES: ϵ_{TH} = Total hemispherical emittance

α_S = Solar absorptance

RCG = Reaction Cured Glass

LI-900 can be easily cut with a band saw or machined. Machining must be performed with diamond-tipped tools because the hardness of the fibers in the material quickly dulls conventional tool cutters.

Table 5 TYPICAL RCG COATING THERMOPHYSICAL PROPERTIES

PROPERTY	VALUE	TEMPERATURE RANGE (°F)
Coefficient of Thermal Expansion, (10^{-6} in./in.°F)	0.57	70 to 1500
	0.56	70 to -100
	0.46	70 to -200
	0.41	70 to -250
Thickness (in.)	0.014	

Table 6 TYPICAL COATING MECHANICAL PROPERTIES AT ROOM TEMPERATURE

PROPERTY	VALUE (psi)
Tensile Strength	4000
Tensile Modulus of Elasticity	4,000,000
Compressive Strengt:.	10000

Lockheed currently produces LI-900 solely for the Space Shuttle program using Government-owned facilities and equipment. Use of these facilities to supply other applications is subject to Government concurrence.

Lockheed Missiles and Space Company
P.O. Box 3504
Sunnyvale, California 94088-3504
(408) 742-4653, 756-7790
January 1987

REFERENCES

1. Grard, R., K. Knott, A.Pederson, *Spacscraft Charging Effects,* Space Science Reviews, Vol. 34, P 289, 1983

2. Heinz, O., R. T. Reaves, *Lithium Ion Emitter for Low Energy Beam Experiments,* The Review of Scientific Instruments, Vol. 39, p 1229, 1968

3. Craven, P. D., R. C. Olsen, J. Fennel, D. Croley, T. Aggson, *Potential Modulation on the SCATHA Spacecraft,* Journal of Spacecraft and Rockets, Vol. 24, p 250, 1987

4. Olsen, R. C., *Experiments in Charge Control at Geosynchronous Orbit _ ATS-5 and ATS-6,* Journal of Spacecraft and Rockets, Vol.22, P 254, 1985

5. Olsen, R. C., *Modification of Spacecraft Potentials by Plasma Emission,* Journal of Spacecraft and Rockets, Vol.18, P 462, 1981

6. Fred M. Johnson, *Studies of the Ion Emitter Beta - Eucryptite,* RCA Review, p 427, 1962

7. Samuel K. Allison, M. Kamegai, *Lithium Ion Sources,* The Review of Scientific Instruments, Vol.32, p 1090, 1961

8. J. P. Blewett. E. J. Jones, *Filament Sources of Positive Ions,* Physical Review, Vol. 50, p 464, 1936

9. James D. Combine, *Gaseous Conductors (Theory and Engineering Applications),* Dover Publications Inc. New York, p 126 - 128, 1958

10. H. B. Haskell, O. Heinz, D. C. Lorents, *Multistage Gun for Production of Low Energy Ion Beams,* The Review of Scientific Instruments, Vol. 37, p 607, 1966

11. M. Remy, R. Process, *A Lithium Ion Source Using the Surface Ionization Process,* The Review of Scientific Instruments, Vol. 41, p 650, 1970

12. Howard L. Daley, Julius Perel, *Lithiun and Sodium Surface Ionization Source Operation and Efficiency,* The Review of Scientific Instruments, Vol. 42, p 1324, 1971

13. R. K. Feeney, Willam E. Sayle, J. W. Hooper, *Aluminosilicate Sources of Positive Ions for Use in Collision Experiments,* Review of Scientific Instruments, Vol. 47 p 964, 1976

14. S.Kita, H. Hubner, W.Kracht, R. Duren, *Beam Source for Moderately Fast Neutral Alkali Atoms,* Review of Scientific Instruments, Vol. 52, p 684, 1981

15. G. Conforti. F.Del Giallo, F. Pietalli, G. Zaccanti, E. D. Anna, G. Leggieri, *An Alkali-Ion Gun for Use in Collision Experiments,* Journal of Physics E: Scientific Instruments, Vol. 15, p 827, 1982

16. D. M. Thomas, W.P. West, K. McCormic, *Low-Divergence, High-Brightness Lithium Ion Source for Plasma Diagnostics,* Review of Scientific Instruments, Vol. 59, p 1736, 1988

17. Data Sheet for LI-900: Lockheed's All-Silica Insulation Material, Lockheed Missiles & Space Company,Inc., Sunnyvale, California, 1987

INITIAL DISTRIBUTION LIST

		No. Copies
1.	Defense Technical Information Center Cameron Station Alexandria, VA 22304-6145	2
2.	Library, Code 0142 Naval Postgraduate School Monterey, CA 93943-5002	2
3.	Physics Library Code Ph Department of Physics Naval Postgraduate School Montery, CA 93943-5000	1
4.	Department Chairman, Code Ph/Wh Department of Physics Naval Postgraduate School Monterey, CA 93943-5000	1
5.	Professor R. C. Olsen, Code Ph/Os Department of Physics Naval Postgraduate School Monterey, CA 93943-5000	10
6.	Professor Otto Heinz, Code Ph/Hz Department of Physics Naval Postgraduate School Monterey, CA 93943-5000	1
7.	Professor S. Gnanalingum, Code Ph/Gm Department of Physics Naval Postgraduate School Monterey, CA 93943-5000	1
8.	Capt. Song, Tae Ik 630-51,Dae-Gu Si, Buk Gu, Pal-dal Dong, 451 Republic of Korea	5
9.	Mr. R. Gracen Joiner Office of Naval Research, Code 1114 800 North Quincy Street Arlington, Virginia 22217-5000	1
10.	Dr. E. C. Whipple Center for Astrophysics and Space Science University of California at San Diego La Jolla, CA 92093	1

11. Dr. C. E. McIlwain — 1
Center for Astrophysics and Space Science
University of California at San Diego
La Jolla, CA 92093

12. Dr. T. E. Moor, ES53 — 1
NASA Marshall Space Flight Center
Huntsville, Alabama 35812

13. Dr. K. Torkar — 1
Institute fur Weltraumforschung Oesterreichische
Akademieder Wissenschaften
Inffeldgasse 12
A - 8810 Graz, Austria

14. Dr. Paul Wilbur — 1
Department of Mechanical Engineering
Colorado State University
Ft. Collins, Colorado 80523

15. Capt. Jung H. Park — 1
SMC 1818, NPS
Monterey, CA 93943

16. Capt. Jong S. Ryoo — 1
SMC 2039, NPS
Monterey, CA 93943

17. Library, P.O. Box 2 — 1
Korea Military Academy
Do-Bong Gu. Gong-Neung Dong 556-21
Seoul, Republic of Korea